Marine and Petroleum Geology 115 (2020) 104289

Contents lists available at ScienceDirect

Marine and Petroleum Geology

journal homepage: www.elsevier.com/locate/marpetgeo

Research paper

Vertical effective stress and temperature as controls of quartz cementation in sandstones: Evidence from North Sea Fulmar and Gulf of Mexico Wilcox sandstones

Olakunle J. Oye[a,*], Andrew C. Aplin[a,*], Stuart J. Jones[a], Jon G. Gluyas[a], Leon Bowen[b], Joseph Harwood[c], Ian J. Orland[d], John W. Valley[d]

[a] Department of Earth Sciences, Durham University, Durham, DH1 3LE, UK
[b] Department of Physics, Durham University, Durham, DH1 3LE, UK
[c] School of Geography, University of Lincoln, Lincoln, LN6 7TS, UK
[d] WiscSIMS Lab, Department of Geoscience, University of Wisconsin, Madison, WI, 53706-1692, USA

ARTICLE INFO

Keywords:
Sandstone
Diagenesis
Quartz cement
Effective stress
Intergranular pressure dissolution
Secondary ion mass spectrometry
Oxygen isotopes

ABSTRACT

We present quantitative petrographic data, high spatial resolution oxygen isotope analyses of quartz cement, basin modelling and a kinetic model for quartz precipitation for two Paleocene-Eocene Wilcox Group sandstones from Texas and two Jurassic Fulmar Formation sandstones from the Central North Sea. At each location, one sandstone has been buried to *ca.* 145 °C and one to *ca.* 185 °C. A key difference between the Wilcox and Fulmar burial histories is that the Wilcox sandstones are currently at higher vertical effective stresses and, from basin modelling studies, have been subjected to generally higher vertical effective stresses through their burial history. The amounts of quartz cement in the Wilcox sandstones are between 12 and 18%, and between 2 and 6% in the Fulmar sandstones. High-spatial-resolution oxygen isotope data obtained from the quartz cements suggest temperature ranges for quartz precipitation from 60 to 80 °C to values approaching maximum burial temperature. Factors such as grain coatings or the timing of petroleum emplacement cannot explain the differences in the amounts of quartz cement. Petrographic data show that most of the silica for quartz cement can be derived from intergranular pressure dissolution. Although the sample set is small, we interpret the results to suggest that the differences in quartz cementation in Fulmar and Wilcox sandstones can be explained better by differences in their vertical effective stress history than their temperature history; in this case, the supply of silica rather than the precipitation of quartz becomes an important control on the rate and extent of cementation.

1. Introduction

Quartz is the volumetrically most important diagenetic cement in sandstones buried to depths greater than 2.5 km (Bjorlykke and Egeberg, 1993; McBride, 1989; Worden et al., 2018a; Worden and Morad, 2000). Quartz cementation occurs as the result of three serially linked processes: the supply of silica; the transport of silica through aqueous solution to precipitation sites; and the precipitation of quartz cement (e.g. Bloch et al., 2002; Taylor et al., 2010; Worden and Morad, 2000). While any of these processes could be the rate-controlling step (e.g. Osborne and Swarbrick, 1999; Oye et al., 2018; Robinson and Gluyas, 1992; Sheldon et al., 2003; Walderhaug, 1996; Worden et al., 2018b; Worden and Morad, 2000), the currently favoured paradigm is that quartz cementation is controlled by the temperature-related kinetics of silica precipitation (Lander and Walderhaug, 1999; Walderhaug, 1996, 2000). In this model, quartz precipitation initiates on geological timescales once a kinetic barrier is broken around 70–80 °C, with the rate increasing exponentially and predictably with temperature (Ajdukiewicz and Lander, 2010; Walderhaug, 1994a, 1996). These ideas have been incorporated into commonly-used models designed to predict quartz cementation and reservoir quality, allowing quartz cementation to be predicted as a function of temperature history (Lander et al., 2008; Lander and Walderhaug, 1999; Taylor et al., 2015; Walderhaug, 2000).

The critical assumption in the temperature-based precipitation model is that silica supply is effectively inexhaustible, so that for each silica molecule precipitated, another is released from a range of potential sources. The most commonly cited and observed silica source is

* Corresponding author.
E-mail addresses: o.j.oye@durham.ac.uk (O.J. Oye), a.c.aplin@durham.ac.uk (A.C. Aplin).

https://doi.org/10.1016/j.marpetgeo.2020.104289
Received 10 September 2019; Received in revised form 22 January 2020; Accepted 7 February 2020
Available online 08 February 2020
0264-8172/

from intergranular pressure dissolution and related stylolitisation at quartz-quartz and quartz-sheet silicate interfaces (Houseknecht, 1988; Osborne and Swarbrick, 1999; Pittman, 1972; Waldschmidt, 1941; Worden and Morad, 2000). In one variant of this model, Bjorkum (1996) proposed that silica is derived from pressure-*in*sensitive dissolution at quartz-mica interfaces, in which case the rate of quartz cementation is controlled uniquely by temperature-related precipitation kinetics.

More commonly, the rate of intergranular pressure dissolution is considered to be primarily a function of vertical effective stress, with a secondary influence of temperature (e.g. van Noort et al., 2008); it occurs at grain contacts because the chemical potential of silica at stressed, grain-grain contacts is enhanced over that in the bulk solution. Gradients in chemical potential drive intergranular pressure dissolution and releases silica which can then precipitate on free detrital quartz surfaces (De Boer et al., 1977; Dewers and Ortoleva, 1990; Elias and Hajash, 1992; Gratier et al., 2005; Oye et al., 2018; Renard et al., 1997; Sheldon et al., 2003; Shimizu, 1995; Tada and Siever, 1989; van Noort et al., 2008). If (a) the silica for quartz cementation was supplied primarily from intergranular pressure dissolution, and (b) supply rather the precipitaition is the rate-controlling step for quartz cementation, we would expect to see a relationship between the extent and rate of cementation with the history of vertical effective stress, rather than temperature. Such a relationship has been proposed previously (Elias and Hajash, 1992; Osborne and Swarbrick, 1999; Sheldon et al., 2003) but rarely tested (Oye et al., 2018).

There are other, local influences on quartz cementation which can complicate the evaluation of the relative importance of silica supply or precipitation as master cementation variables. Grain-coating clay and microquartz reduce the availability of precipitation sites on quartz grains, inhibiting cementation and preserving porosity (Aase et al., 1996; Ajdukiewicz et al., 2010; Bloch et al., 2002; French et al., 2012; Gluyas et al., 1993; Heald and Larese, 1974; Osborne and Swarbrick, 1999; Stricker and Jones, 2016; Stricker et al., 2016). Furthermore, although debate continues, there is some consensus that the occurrence of hydrocarbons slows the rate of quartz cementation by altering the wetting state of grains and/or increasing the tortuosity of diffusion pathways (Maast et al., 2011; Marchand et al., 2000, 2001, 2002; Sathar et al., 2012; Worden et al., 2018b).

The aim of this paper is to consider the relative importance of (a) silica supply by intergranular pressure dissolution, and (b) silica precipitation as controls on quartz cementation. In an earlier paper, Oye et al. (2018) described the anomalously low volumes of quartz cement in sandstones from the North Sea's High Pressure High Temperature Elgin Field, suggesting that it may be the history of effective stress rather than the history of temperature which is a key control on quartz cementation. Here, we extend that study and test its findings more robustly by studying four carefully selected sandstones that have different vertical effective stress and temperature histories. Two were chosen from Upper Jurassic Fulmar Formation sandstones from Clyde and (the previously studied) Elgin Fields in the Central North Sea (CNS), UK, and two from Paleocene-Eocene Wilcox Group sandstones from Rotherwood and Lake Creek Fields in the Texas coast, Gulf of Mexico (GoM), USA (Fig. 1); Elgin and Rotherwood have lower present-day vertical effective stress and higher temperatures than their equivalents from Clyde and Lake Creek (Table 1). Our approach is to integrate (a) quantitative petrographic analysis, (b) basin modelling to evaluate temperature and vertical effective stress histories, (c) high-spatial-resolution oxygen isotope analyses to evaluate quartz cementation histories and (d) kinetic modelling of quartz cementation.

2. Geological settings

Samples were selected from four locations, two from the UK North Sea and two from the Texas Gulf Coast, enabling us to examine the relative importance of both temperature and vertical effective stress on quartz cementation (Table 1). For the chosen Formations, Elgin (North Sea) and Rotherwood (Texas) have current temperatures of 185–189 °C but different vertical effective stress, and Clyde (North Sea) and Lake Creek (Texas) have temperatures of 143–147 °C, again with different vertical effective stress.

Samples from Elgin and Clyde Fields were taken from the syn-rift Upper Jurassic Fulmar Formation in the Central Graben area of the UK North Sea (Fig. 1). The Upper Jurassic Fulmar Formation is one of the principal hydrocarbon reservoirs in the UK Central Graben (e.g. Gilham et al., 2005; Gowland, 1996; Kuhn et al., 2003; Lasocki et al., 1999; Osborne and Swarbrick, 1999; Stevens and Wallis, 1991; Wilkinson and Haszeldine, 2011; Wilkinson et al., 2006). Sediments were probably sourced from the Triassic sedimentary rocks of the Western Platform in the Central North Sea, with some contributions from intrabasinal highs such as the Forties – Montrose High and Josephine ridge (Gowland, 1996). The Fulmar Formation is a shallow marine sandstone, intensely bioturbated and often occurring as a coarsening-upward succession grading from siltstones into very fine to medium grained arkosic sandstones (Gowland, 1996; Hendry et al., 2000; Lasocki et al., 1999). The Fulmar Formation is mainly Oxfordian to Kimmeridgian in age, but its geographic variability and diachroneity resulted in the occurrence of localised areas of the Fulmar Formation with younger ages that extend to Ryazanian times (Fig. 2). The presence of abundant *Rhaxella* sponge spicules has been reported within some intervals, locally (Gowland, 1996). The Fulmar Formation is buried beneath a thick Upper Jurassic to Tertiary succession of chalk, clays and silts.

Samples from the upper Texas Gulf Coast were taken from the Late Paleocene to Early Eocene, fluvio-deltaic Wilcox Group (Figs. 1 and 3 (Dutton and Loucks, 2010; Fisher and McGowen, 1967; Galloway et al., 2000)). Wilcox Group sediments comprise a series of sandstones, siltstones and shales which have been extensively studied (Dutton and Loucks, 2010; Fisher and McGowen, 1967; Galloway et al., 2000). Sediments were likely sourced from the Laramide uplands area in the southern Rocky Mountains. Most Wilcox sandstones in the upper Texas coast are lithic arkoses and feldspathic litharenites (Dutton and Loucks, 2010). Because geothermal gradients vary in the Texas coast area from 24 to 43 °C/km, the Wilcox sandstones exhibit varying temperature regimes across different localities (Dutton and Loucks, 2010).

3. Methods

3.1. Sampling strategy

A key objective of this paper is consider the relative importance of effective stress and temperature histories as controls on quartz cementation in sandstones. Since other factors, some of which vary on small spatial scales, also influence the amount of quartz cement (grain-coating clay, early carbonate cement, grain-coating microquartz, hydrocarbon fill in the porosity), our sampling strategy here was to obtain a relatively small number of samples with a limited range of detrtial mineralogy and grain size. Restricting the influence of other variables allows greater insights into the importance of effective stress and temperature histories. Furthermore, our aim to constrain quartz cementation histories based on oxygen isotope microanalysis using secondary ion mass spectrometry, inevitably restricts the number of samples which can be characterised in detail.

Fulmar Formation samples were obtained from wells 30/17b-2 and 22/30c-G4 in Clyde and Elgin Fields respectively (Fig. 1), from clean, clay-poor intervals (Table 1). A similar strategy was adopted for the Wilcox sandstones: two wells that penetrated the Wilcox sandstones were selected, one from Mobil #48 well in Lake Creek Field, Montgomery County, and one from Texaco #1 well in Rotherwood Field, Harris County, Texas. All the sandstones are at or close to their maximum burial depth. Sample depths, temperatures and vertical effective stress are given in Table 1.

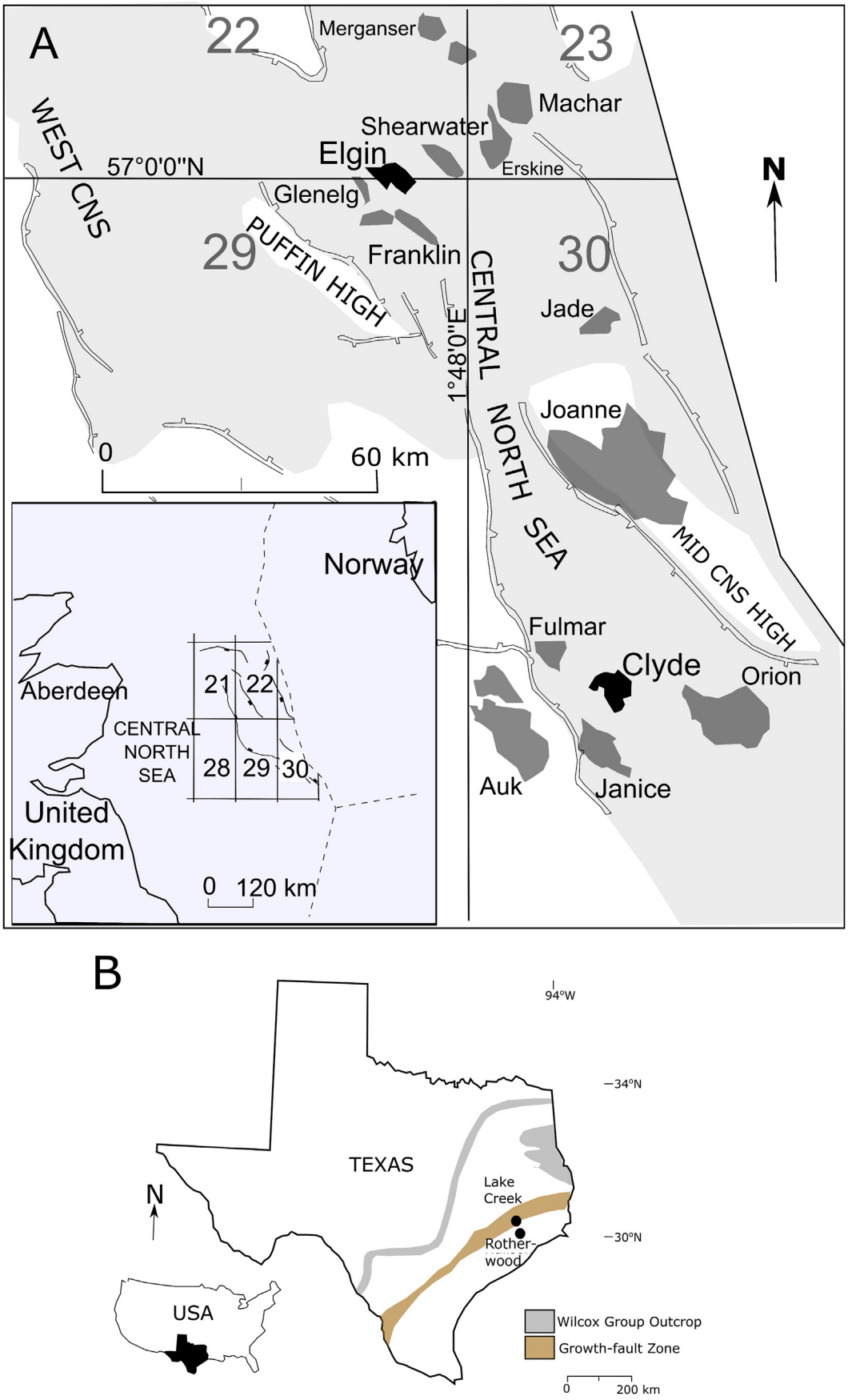

Fig. 1. Maps of study locations; A) UK Central North Sea (CNS) showing Clyde, Elgin and other surrounding fields: B) Texas showing Lake Creek Field in Montgomery County and the Texaco No. 1 Hallson Well, Rotherwood Field in Harris County (Adapted from Fisher and Land (1986) and Day-Stirrat et al. (2010)).

Table 1
Depth, Vertical Effective Stress and Temperature matrix for the studied Fulmar Formation and Wilcox Group sandstones.

Field	Basin	Group/Formation	Age	Depth (m ssTVD)	Temp (°C)	VES (MPa)
Clyde	UK Central North Sea	Fulmar	Upper Jurassic	3770–3790	147	40.0
Elgin	UK Central North Sea	Fulmar	Upper Jurassic	5410–5435	189	12.3
Lake Creek	Gulf of Mexico	Wilcox	Early Eocene	3518	143	33.4
Rotherwood	Gulf of Mexico	Wilcox	Paleocene-Eocene	5063	185	23.9

3.2. Petrography

Petrographic data for the Wilcox sandstones were obtained from Harwood (2011), except intergranular pressure dissolution data which were measured in this study. Fulmar Formation sandstones were characterised using standard and cathodoluminescence (SEM-CL) petrography. Using a standard petrographic microscope, grain types, matrix and cement contents were quantified by making not less than 300 point counts per thin section. This revealed that some Fulmar samples contained early carbonate cement. These carbonate cement-rich samples were excluded from further analyses, since early carbonate can significantly occlude porosity and thus bias quartz cement results (Oye, 2019). Twenty Fulmar samples (Table S6), representing the full range of quartz cement abundance, were subsequently selected for CL petrography. The CL petrography involved the acquisition of Si element and CL maps over the same areas (3 mm × 3 mm) for each of the twenty thin sections using energy dispersive X-ray (EDX) and SEM-CL. A grid of 1600 (40 × 40) square boxes was superimposed on the CL map, while the EDX map was used as a control for the identification of mineral grains. Modal analysis was then performed by manually point-counting detrital quartz, dissolved quartz along grain contacts and authigenic quartz using the grids to generate 1600 data points per thin section. Cathodoluminescence petrography allows discrimination of original grains and cements, so that initial grain sizes were estimated by measuring the diameter of ~120 grains each from ten Fulmar thin-sections. A more detailed CL petrography method is described in the supplementary material.

3.3. Effective stress and temperature histories

One-dimensional basin modelling was used in this study to reconstruct the burial, pore pressure, effective stress and temperature histories for both Fulmar Formation and Wilcox Group sandstones using Schlumberger's PetroMod Petroleum Systems modelling software (Version 2014.1).

Stratigraphic data from composite logs, geological well reports, core analysis, and core description reports were used to create the models (Tables S1, S2 and S3). Drill Stem Test (DST) temperature data for

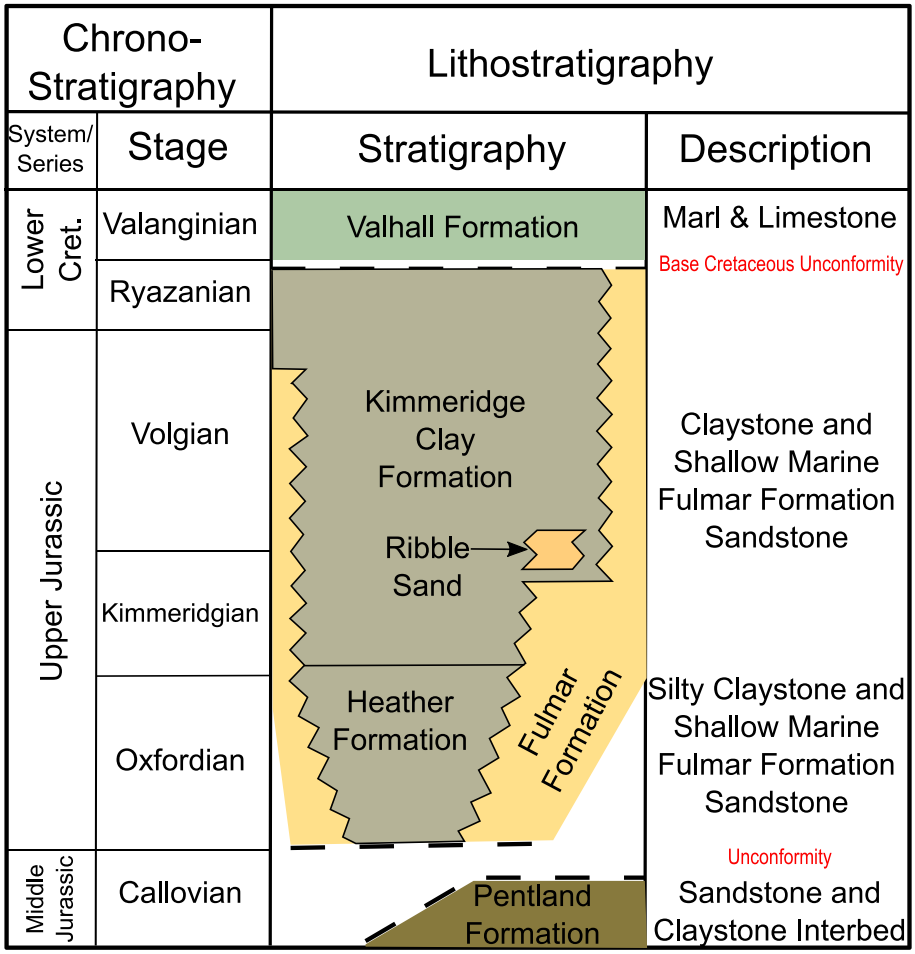

Fig. 2. Regional stratigraphy of the Central North Sea from Middle Jurassic to Lower Cretaceous. Shallow marine Fulmar Formation was investigated in this study (adapted from Graham et al., 2003)

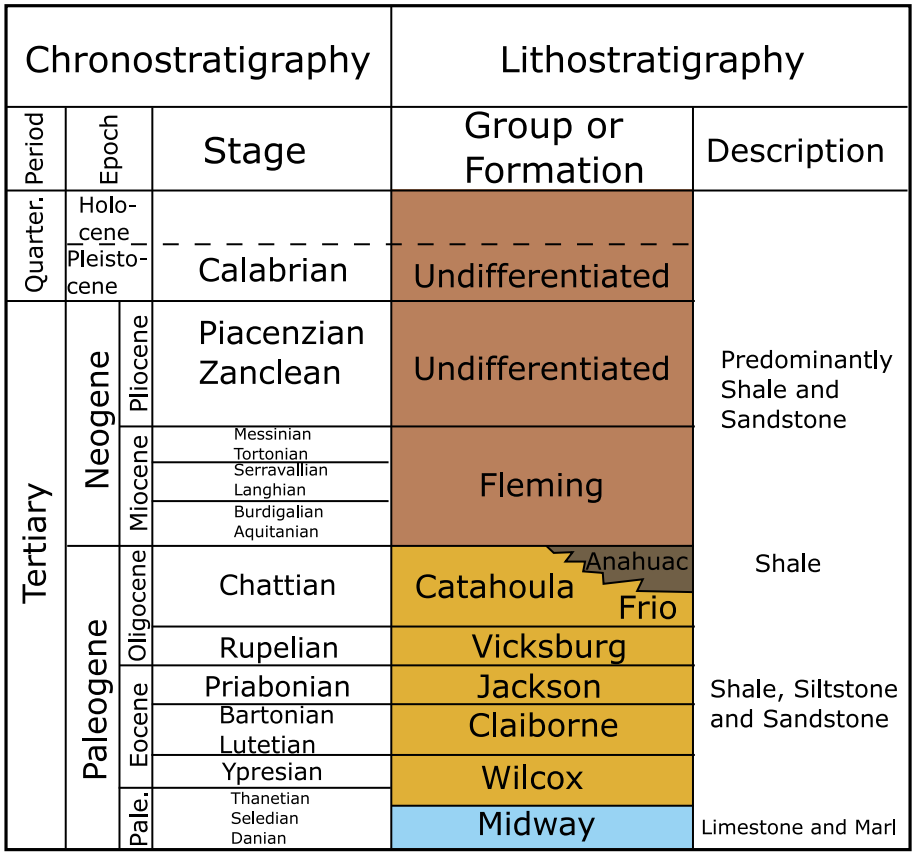

Fig. 3. Generalised stratigraphy of the Gulf Coast Tertiary and Quaternary section showing the Paleocene-Eocene Wilcox Group and other formations (adapted from Pitman and Rowan, 2012).

Clyde Field obtained from well composite log and corrected bottom-hole temperature (BHT) data for Elgin Field were obtained from unpublished well reports. Historical mean surface temperatures were estimated using a PetroMod inbuilt algorithm that relates global mean surface temperatures with paleolatitudes and geologic ages. Heat flow models were built after Allen and Allen (1990), with an average of 62 and 64 mW/m^2 for Elgin and Clyde Fields through the basin's history. The heat flow values at the peak of Permo-Triassic and Upper Jurassic paleo-rifting events were 70 and 90 mW/m^2 respectively for both Elgin and Clyde Fields. Heat flow, however, averages ~57 mW/m^2 (range 50–78 mW/m^2) for fields in the Gulf of Mexico (Nunn and Sassen, 1986; Smith et al., 1981). Vitrinite reflectance data (only available for the Fulmar sandstones) were used as paleothermometers and combined with present-day temperature data to constrain thermal models and reconstruct temperature evolution through time (Figs. S1, S2, S3 and S4).

For the fluid flow part of the basin modelling, lithological data for each sedimentary unit were defined in Clyde and Elgin Fields from well composite logs and core analysis descriptions, while the lithologies for Lake Creek and Rotherwood Fields were solely based on log data. Petromod's default lithologies were modified to match those observed in field samples. Pore pressure data obtained from field measurements were used to constrain the pore pressure model for reconstruction of effective stress histories for all the fields. The calculation of vertical effective stress is based on the mathematical expression of Terzaghi (1925):

$$\sigma_v = S_v - P \quad (1)$$

where σ_v is vertical effective stress, S_v is vertical lithostatic stress and P is pore fluid pressure (all in Pa).

Default chalk and shale permeabilities in PetroMod were modified after Swarbrick et al. (2000), lowering permeabilities for the Chalk Group and the Pre-Cretaceous shale units until a good fit was achieved between modelled and observed pore pressures. The Chalk group were assigned typical shale permeability values because they are extensively cemented (Swarbrick et al., 2000, 2010). Similar adjustments were made for Rotherwood and Lake Creek Fields, where permeability values for the Claiborne and Wilcox shales were modified to lower values (nanoDarcies) until modelled pore pressures matched field data.

Although temperature histories can be quite accurately modelled in 1D, the same is not necessarily true for pore pressure and vertical effective stress, since one-dimensional modelling packages are limited by their inability to model lateral fluid flow. It transpires that this is critical for the Clyde Field, where regional pore pressure data within the Fulmar Formation show that pore fluid pressures have decreased substantially in the last *ca.* 0.5 million years as a result of lateral drainage (Swarbrick et al., 2005). These data strongly suggest that vertical effective stress has increased from *ca.* 19 MPa 0.5 million years ago, to 40 MPa at the present-day. This is critical for the present study, given its focus on unravelling the relative importance of temperature and effective stress on quartz cementation.

3.4. Kinetic model of quartz cementation

Quartz cementation models were built using Walderhaug (1996) approach, which simulates the precipitation of silica on quartz surfaces as a logarithmic function of temperature. Commercial quartz cementation modelling software packages based on the Arrhenius equation have also been developed (e.g. Lander et al., 2008; Walderhaug, 2000; Walderhaug et al., 2000) but were not available for this study. However, the essential inputs for each model - a time-temperature history and the surface area of macroquartz grains - are the same. The key difference is that in the Walderhaug (1996) model, the kinetics of

precipitation are defined by a logarithmic function, whereas in the Arrhenius approach, the kinetics are defined by the pre-exponential factor and activation energy terms in the Arrhenius equation. In both cases, key kinetic parameters can be adjusted to obtain local calibrations to quartz cement abundances. Local calibration is not the aim here; rather, we use single values of the key kinetic constants in Walderhaug (1996) equation to observe the extent to which a general model can match observed amounts of quartz cement in different settings. Whilst the Arrhenius approach to the quantification of quartz precipitation may have a more robust scientific basis, we note that Arrhenius and logarithm-based methods yielded similar results for some Jurassic Brent Group sandstones from the North Sea (Walderhaug, 2000).

Walderhaug (1996) empirical model is mathematically expressed as:

$$Vq_2 = \Phi_0 - (\Phi_0 - Vq_1)\exp\frac{-MaA_0}{\rho\Phi_0 bc\ \ln 10}(10^{bT_2} - 10^{bT_1}) \quad (2)$$

where M and ρ are molar mass (60.09 g/mol) and density (2.65 g/cm^3) of quartz; c is the heating rate (°C/s) calculated from time-temperature history; Φ_0 is the porosity at the onset of precipitation; Vq_1 is the volume (cm^3) of quartz cement present in 1 cm^3 of sandstone at time T_1 (s); Vq_2 is the volume (cm^3) of quartz cement precipitated in 1 cm^3 of sandstone from time T_1 and T_2 (s); A_0 is initial quartz surface area (cm^2) in 1 cm^3 of sandstone (estimated from grain size); and a (moles/cm^{2}s) and b (°C^{-1}) are the precipitation kinetic constants (Walderhaug, 1996).

Through the quartz surface area term, the model incorporates grain size, mineralogy, and available quartz surface area, all of which were quantified in this study. The model assumes that compaction terminates at the onset of quartz cementation, at which point the sandstone framework is stabilised. Time-temperature histories generated from Petromod were used to calculate the heating rates incorporated in the cementation models. The model used 1 cm^3 sandstone, an 80 °C threshold temperature for cementation, 26% porosity at the onset of quartz cementation, grain size estimates from thin-sections during CL petrography, and Walderhaug (1994b) kinetic constants a (1.98×10^{-22} mol/cm^{2}s) and b (0.022°C^{-1}). Fractions of detrital quartz in the bulk rock were obtained from CL petrographic data. Quantitative petrographic data of grain coat coverage were also incorporated in the model using a method similar to Walderhaug (1996) and (Walderhaug, 2000) approach, for a better constraint of the available quartz surface area. Quantification of grain coatings coverage was done through visual inspection and manual point counting using cathodoluminescence, back-scattered electron, and silica maps generated over the same area (Oye et al., 2018; Oye, 2019). While back-scattered electron microscopy allowed the identification of microquartz and clay coatings in thin section, cathodoluminescence and silica maps helped identify and discriminate quartz grains and cement.

3.5. Oxygen isotope analysis

One sample was selected from each of Clyde and Elgin Fields for *in situ* oxygen isotope analysis of quartz overgrowths, using a CAMECA IMS-1280 ion microprobe at the WiscSIMS Laboratory at the University of Wisconsin-Madison (Kelly et al., 2007; Kita et al., 2009; Valley and Kita, 2009). Six overgrowths with thicknesses between 40 and 100 μm, three from each sandstone sample, were chosen for analysis. Linear profiles of $\delta^{18}O$ were measured across each overgrowth using a 3 μm spot diameter. Individual samples were embedded in a polished epoxy mount alongside grains of University of Wisconsin quartz standard UWQ-1 (Kelly et al., 2007). Bracketing analyses were performed on the quartz standard grains within each of the mounts to enable correction of measured $\delta^{18}O$ values to the Vienna Standard Mean Ocean Water (VSMOW) scale. Normally, eight UWQ-1 analyses bracketed each group of ~12 sample analyses to monitor instrumental drift and to calculate external reproducibility for sample analyses (Kita et al., 2009; Valley and Kita, 2009). The average spot-to-spot reproducibility of $\delta^{18}O$ in the bracketing UWQ1 analyses was 0.7‰ (2 standard deviations).

Ion microprobe analysis of individual quartz overgrowths in Wilcox and Fulmar sandstones were similar except that measurements in the Wilcox sandstones were made using a 12 μm spot size, which improved spot-to-spot reproducibility to 0.7‰ (2 standard deviations). In addition, $16OH^-$ was measured simultaneously during $\delta^{18}O$ analysis of the Fulmar samples. Ratios of $16OH^-/16O^-$ were background-corrected by subtraction of average ratios measured on nominally anhydrous UWQ-1 analyses that bracketed each block of sample data. Four analyses representing outlying data points after $16OH^-/16O^-$ correction were discarded (Fig. S4 and Fig.S5). A more detailed ion microprobe analytical procedure is described in prior studies (Kita et al., 2009; Oye et al., 2018; Page et al., 2007; Pollington et al., 2011; Valley and Kita, 2009). All data are reported in the supplementary material (Tables S8 and S9).

4. Results

4.1. Burial, temperature and vertical effective stress histories

Burial histories are shown in Fig. 4, and both temperature and vertical effective stress histories in Fig. 5. Temperature histories for Clyde and Elgin Fields are broadly similar, with higher temperatures in Elgin as a result of a more rapid early phase of burial (Fig. 5). Temperature histories for Rotherwood and Lake Creek Fields are also like each other, with higher temperatures in Rotherwood Field due to greater burial in the Eocene-Oligocene (Fig. 5).

In Rotherwood and Lake Creek Fields, vertical effective stress increases rapidly in the first 10–20 million years as a result of the rapid burial of a relatively coarse-grained sedimentary sequence which allows the effective dissipation of fluid overpressure (Fig. 5). Vertical effective stress is then fairly constant until the present-day. Although the Wilcox Group at Lake Creek Field is less deeply-buried than at Rotherwood Field, vertical effective stress is higher as fluid pressure is much lower, reflecting the more rapid burial at Rotherwood Field and the relative inability of the sediment sequence to dewater and thus lose pore

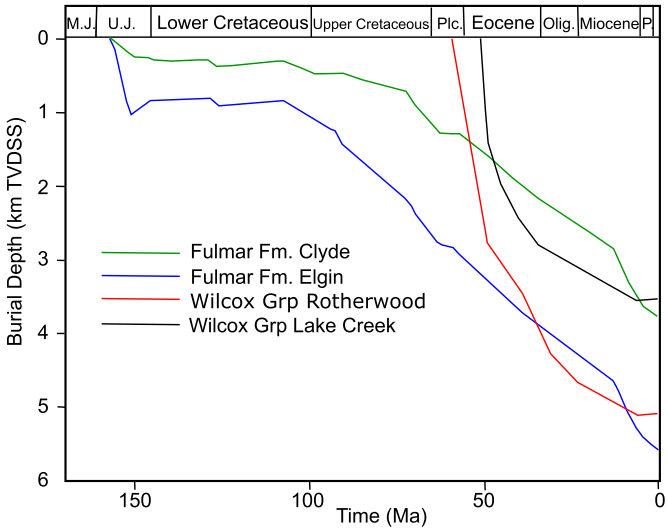

Fig. 4. Burial history reconstruction for the Central North Sea Fulmar Formation sandstones from Clyde and Elgin Fields, and the onshore Gulf of Mexico Wilcox Group sandstones from Rotherwood and Lake Creek Fields. These models were constructed by using a forward modelling approach on PetroMod 1D version 2014.1. Fulmar Formation sandstones are 100Myrs older than the Wilcox Group sandstones. M.J – Middle Jurassic, U.J – Upper Jurassic, Plc – Paleocene, Olig. – Oligocene, P. – Pliocene, TVDSS – True vertical depth subsea.

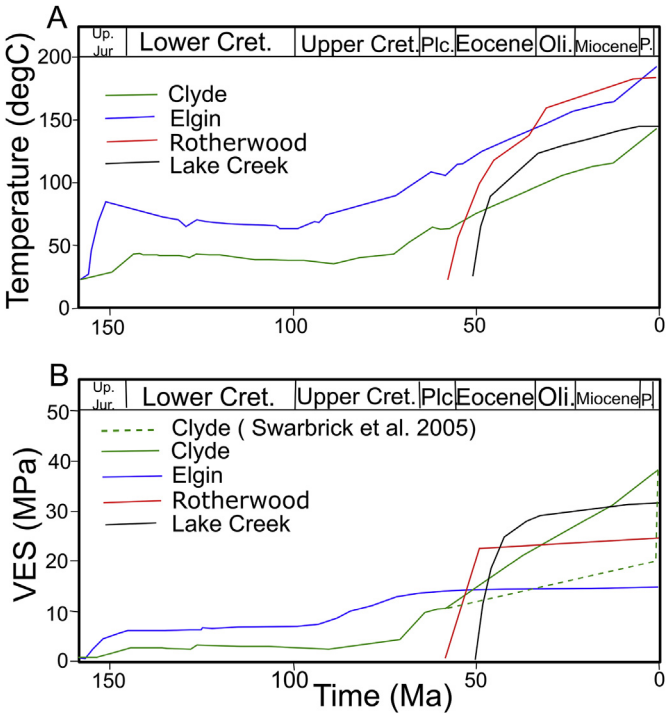

Fig. 5. Modelled temperature (A) and vertical effective stress (B) histories for Central North Sea Fulmar Formation from Clyde and Elgin Fields, and Gulf of Mexico Wilcox sandstones from Rotherwood and Lake Creek. These models were constructed by using a forward modelling approach on PetroMod 1D version 2014.1. Upper Jurassic Fulmar Formation sandstones are 100 Ma older than the Paleocene-Eocene Wilcox Group sandstones. Green dashed line represents the most likely evolution pathway for Fulmar Formation vertical effective stress history in Clyde Field based on Swarbrick et al. (2005) Fulmar Formation sandstones experienced low vertical effective stress (VES) for most of their burial histories compare to Wilcox Group sandstones. (For interpretation of the references to colour in this figure legend, the reader is referred to the Web version of this article.)

pressure at the same rate as it is being generated by additional sediment loading.

Vertical effective stress is low in the Fulmar Formation throughout the burial history of Elgin Field, and was never greater than the present 12 MPa (Fig. 5). This is due to the fine-grained nature and low permeability of most of the overburden above the Fulmar sandstones (See Supplementary Material). Since the stratigraphic column at Clyde Field is like that at Elgin, the evolution of vertical effective stress should be similar to that at Elgin, perhaps with slightly higher vertical effective stress due to a lower burial rate and thus the greater possibility of pore pressure dissipation by fluid flow. However, the present-day vertical effective stress is much higher than that at Elgin, 40 MPa rather than 12 MPa (Table 1). As discussed earlier, regional studies of the Fulmar Formation in the Clyde area show pore pressure distributions which indicate regional depressurisation of the Fulmar sandstones through a leak point well to the west of Clyde (Swarbrick et al., 2005). The regional pore pressure data are best interpreted as depressurisation occurring over the last 0.5 million years, increasing the vertical effective stress at Clyde from 19 MPa to 40 MPa (Swarbrick et al., 2005). Vertical effective stress at Clyde is likely to have been low, no more than 19 MPa, throughout all of its burial history bar the last 0.5 Ma.

4.2. Petrographic observations

The two Wilcox sandstone samples from Rotherwood and Lake Creek Fields are clean, fine grained, lithic sub-arkose sandstones, with higher plagioclase fractions than their Fulmar Formation counterparts (Fig. 6; Table 2 and Table 3). Average porosities in the examined samples are 6.8% for the sample from the Texaco #1 Hallson well in Rotherwood Field and 11.8% for the sample from the Mobil #48 well in Lake Creek Field (Table 3). The feldspars have experienced large scale albitization and dissolution (Dutton and Loucks, 2010). Grain-replacing-ankerite cements were observed only in the sample from the higher-temperature Rotherwood Field (Fig. 6E).

The Upper Jurassic Fulmar Formation sandstones investigated in this study were selected from clay-poor, upper shoreface facies in Clyde and Elgin Fields. They are fine grained, with subangular to subrounded grains, and an arkosic mineralogical composition. Illite, the main authigenic clay type observed in these sandstones, is generally less than 3% of bulk composition in all thin sections (Table 2). These clays most likely have both detrital and authigenic (product of feldspar dissolution) origins and are found as grain coats or pore-filling matrices. The illite grain coats in Elgin Field are also found coating authigenic quartz, and the matrices are frequently impregnated with bitumen (Fig. 7). Partially or completely dissolved feldspars, with their initial shape preserved as hollow clay rims, are common features in the Elgin field, but infrequently observed in Clyde Field. Intragranular porosity, which is the measure of dissolved feldspars in the analysed thin sections, averages 0.9% in Clyde and 3.3% in Elgin (Fig. 7E and F; Table 2). Intragranular porosity from feldspar dissolution was probably underestimated in Clyde samples, as oversized intergranular pore spaces which are most likely sites of dissolved grains are present in the samples. Carbonate cements are around 9% in the Fulmar sandstone samples from both fields (Table 2). These carbonates are often found occluding available pore spaces or destroying porosity locally. Some carbonates were also found as replacive cements in Elgin samples, where they either partially or completely replace dissolved mineral grains. Mineralogically, these carbonate cements occur as discrete dolomite, ferroan dolomite, and as ferroan dolomites surrounding dolomite cores. In addition to dolomite and ferroan dolomites, syntaxial ankerite rims on dolomite nuclei were commonly observed in Elgin samples. Lithic fragments, micas and pyrite are the other minor components common to samples from both fields, with glauconite observed only in Clyde.

4.2.1. Quartz cementation

Two types of quartz cements, macroquartz and microquartz, were observed by qualitative petrographic analysis (Figs. 7, 8 and 9). The macroquartz cements occur as syntaxial and blocky overgrowths and are optically continuous with their detrital quartz nuclei under transmitted light. Different cathodoluminescence zoning patterns can be observed within some of the macroquartz overgrowths at high resolution (Fig. 8). In contrast, microquartz overgrowths are thin, randomly oriented, polycrystalline quartz overgrowths, with lengths usually ranging from 1 to 10 μm (Aase et al., 1996; French and Worden, 2013).

Quantitative cathodoluminescence petrographic data from the Central North Sea samples (Table 2) show sandstones from Elgin and Clyde Fields have similar volumes of macroquartz cement (4.6% and 4.4% respectively). However, normalization of macroquartz cement volume to detrital quartz content, which is required to avoid bias resulting from variations in the detrital mineralogical composition of the samples (see Houseknecht, 1984, 1988, 1991), indicates that Clyde samples have 20% more macroquartz cement than Elgin samples (Table 2).

For the Gulf of Mexico Wilcox Group, the sample from Lake Creek Field has macroquartz cement content of 18.8% compared with 12.3% in the higher temperature Rotherwood samples. Although this study only investigated two samples from the Wilcox Group sandstones, the high volume of quartz cement measured in this study is comparable to the average 12 vol % measured by (Grigsby et al., 1992) from forty-six Wilcox Group sandstones from Lake Creek Field. After normalization to detrital quartz content, the Lake Creek sample has 37% more macroquartz cement than the sample from Rotherwood Field (Table 3). The

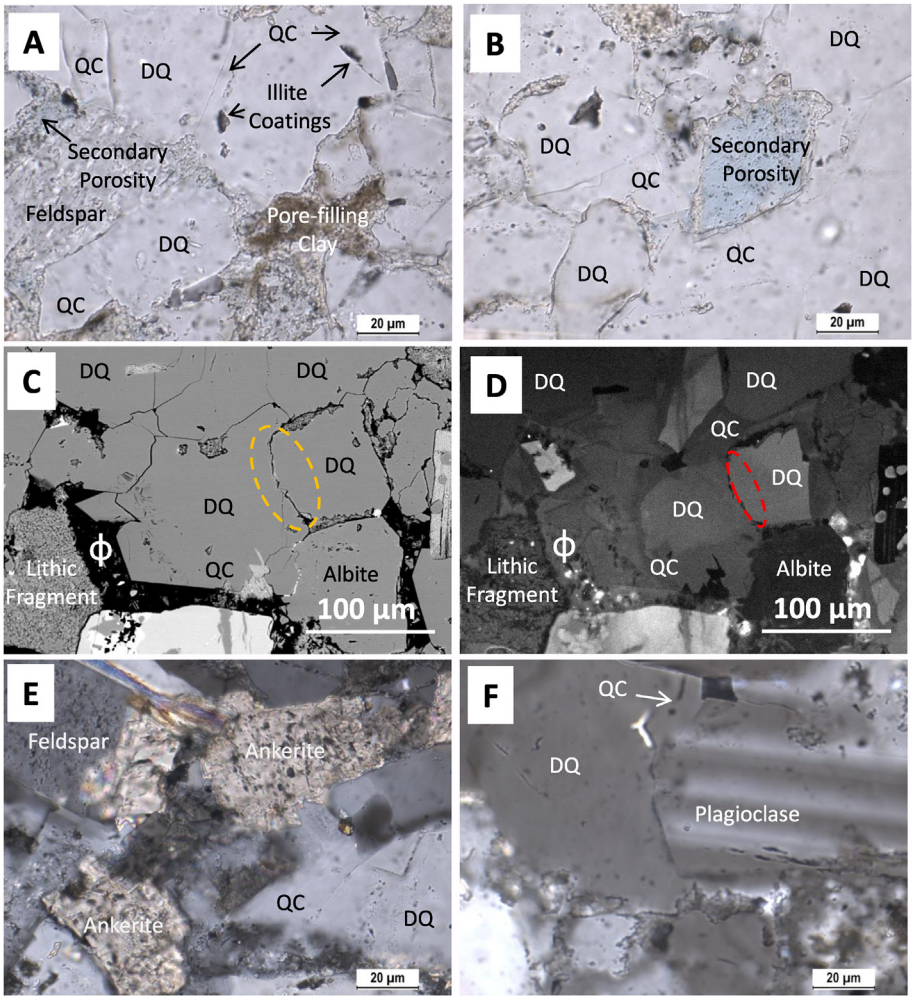

Fig. 6. A) Optical thin-section photomicrograph (plane polarized) of Wilcox sandstone sample from Lake Creek Field showing interlocked mineral grains, pore-filling illite, and grain-coating illite engulfed by quartz cement (QC). Detrital quartz is represented by DQ. B) Optical thin-section photomicrograph (plane polarized) of Wilcox sandstone of Lake Creek Field samples showing secondary porosity from dissolved feldspars. C) Back-scattered electron (BSE) image of Wilcox sandstone sample from Lake Creek Field. The region enclosed in orange circle shows intergranular pressure dissolution. D) Equivalent cathodoluminescence (CL) image of slide C showing example of projected grain boundary (red circle) used for quantification of intergranular pressure dissolution (after Sibley and Blatt (1976) and Houseknecht (1991)). E) Optical thin-section photomicrograph (cross polarized) of Wilcox sandstone sample from Rotherwood Field showing ankerite cement replacing grains (presumably feldspars) in sandstones from Rotherwood Field are visible in cross polarized light image (F). Optical thin-section photomicrograph (cross polarized) of Wilcox sandstone sample from Rotherwood Field showing plagioclase feldspar. Plagioclase feldspars are more common in Wilcox Group sandstones than their Fulmar Formation counterparts. (For interpretation of the references to colour in this figure legend, the reader is referred to the Web version of this article.)

studied Wilcox samples have at least 40% more macroquartz cement than the Fulmar Formation samples at equivalent temperatures.

In all cases, observed macroquartz cement volumes in these Fulmar Formation and Wilcox Group sandstones are lower than those predicted by the quartz cementation model (Table 4; Fig. 11). Modelled quartz cement volumes can always be matched to observed volumes by changing the precipitation kinetic constants a and b in equation (2). However, very different values of a and b are needed in each of the four cases, implying that cementation is not a unique function of temperature. The same conclusion would be drawn if Arrhenius-based kinetics were used to model quartz cement; it would be possible to alter the pre-exponential factor and activation energies within the equation to obtain a local calibration to the amount of quartz cement, but very different constants would be needed to model the quartz cement volumes in the North Sea sandstones compared to the Gulf of Mexico sandstones. Given the relative simplicity of the quartz precipitation reaction, one might expect the kinetic constants to be similar in all situations.

Microquartz was frequently observed within certain intervals in the Clyde samples where they occur as well developed, and sometimes pore-occluding overgrowths, but are almost absent in Elgin samples (Figs. 7 and 9). No microquartz was observed in the Wilcox sandstones, as in previous studies (e.g. Dutton and Loucks, 2010; Grigsby et al., 1992; McBride et al., 1991).

4.2.2. Intergranular pressure dissolution

Estimation of intergranular pressure dissolution along grain contacts was performed on cathodoluminescence images using Sibley and Blatt (1976) and Houseknecht (1991) approach (Figs. 6D and 8A). Grain boundaries were projected along grain contacts where dissolution has taken place (Figs. 6D and 8A), and the inferred features were point-counted as percentage volumes of silica dissolved by intergranular pressure dissolution. Quantitative results suggest that the average volume of silica released by intergranular pressure dissolution is 2.7% in Clyde, 2.7% in Elgin, 11.7% in Rotherwood and 19.7% in Lake Creek (Tables 2 and 3). Normalization of grain loss to detrital quartz content (see Houseknecht, 1984, 1988, 1991) (shows that approximately 20% more silica is released by intergranular pressure dissolution in the Fulmar Formation samples from Clyde Field than in higher temperature, low vertical effective stress samples from Elgin Field (Table 2). Similar observations were made for the Wilcox Group samples, where approximately 40% more silica is released by intergranular pressure dissolution in the sandstone samples from Lake Creek Field than in the higher temperature, lower vertical effective stress sample from Rotherwood Field (Table 3). Inter-basinal comparison of the normalised data also shows that at equivalent temperatures, > 45% more silica is released by intergranular pressure dissolution in the studied Wilcox Group sandstones than their Fulmar Formation counterparts.

In summary, while accepting that this is a small set of sandstones, the combined results from the four fields (Table 5; Fig. 5; Fig. 12) suggest that:

a) There is a strong positive relationship between the extent of intergranular pressure dissolution and the amount of quartz cement. Most of the quartz cement can be supplied via intergranular pressure dissolution, with additional silica from feldspar dissolution.
b) At a given temperature, when normalised to detrital quartz, there is

Table 2
Petrographic data of the Upper Jurassic Fulmar Formation sandstones from Clyde and Elgin fields, Central North Sea. Number of analysed samples is the same for the two fields. More detailed data are reported in the supplementary material (Fig. S3; Tables S4, S5, S6 and S7).

	Number of samples	Clyde Mean	Clyde Standard Deviation	Clyde Minimum	Clyde Maximum	Elgin Mean	Elgin Standard Deviation	Elgin Minimum	Elgin Maximum
Detrital grain size (mm)	10	0.18	0.06	0.06	0.41	0.16	0.05	0.06	0.36
Quartz (%)	19	38.1	3.9	30.3	44.3	44.2	5.6	32.3	55.7
Feldspar (%)	19	27.3	3.3	19.7	32.7	23.5	3.4	17.3	29.7
Lithic Fragments (%)	19	1.2	0.5	0.0	2.3	1.1	0.7	0.0	2.7
Quartz cement - standard petrography (%)	19	3.6	1.6	0.7	7.0	2.0	1.4	0.3	6.3
Quartz cement - CL petrography (%)	10	4.4	1.1	2.7	5.9	4.6	1.2	2.1	6.4
Intergranular Pressure Dissolution - CL petrography (%)	10	2.7	1.0	1.1	3.8	2.7	0.8	1.4	3.8
Quartz cement normalised to detrital quartz	10	0.15	0.03	0.10	0.20	0.12	0.03	0.05	0.15
Intergranular Pressure Dissolution normalised to detrital quartz	10	0.09	0.03	0.04	0.13	0.07	0.02	0.04	0.10
Carbonate cement (%)	19	8.7	5.1	1.3	21	9.4	12.3	0.0	40
Intergranular porosity (%)	19	12.9	2.7	7.3	17.0	11.0	4.6	1.7	20.7
Intragranular porosity (%)	19	0.9	1.0	0.0	3.0	3.3	1.5	1.0	8.0
Core Porosity (%)	33	24.4	2.1	17.2	29.4	22.0	5.2	8.5	27.9
Authigenic and detrital clay (%)	19	2.3	1.4	0.3	5.3	2.8	2.3	0.7	9.3

much more quartz cement in the Wilcox sandstones than the Fulmar sandstones.

c) The Fulmar sandstones in this study have been subjected to much lower effective stresses through most of their history, compared to the Wilcox sandstones.

4.2.3. Oxygen isotope composition of macroquartz cements

High resolution SIMS analysis has proven to be a valuable tool for reconstructing cementation histories of diagenetic quartz cement, by measuring $\delta^{18}O$ profiles across individual macroquartz overgrowths (e.g. Denny et al., 2019; Harwood et al., 2013; Pollington et al., 2011).

Seventy-two $\delta^{18}O$ measurements were made on six different overgrowths from two sandstones from Clyde and Elgin sample sets. All $\delta^{18}O_{(qc)}$ results are shown as a function of the distance from their detrital grain boundary in (Fig. 10). Values of $\delta^{18}O_{(qc)}$ in the Fulmar sandstone sample from Clyde shows a 4.1‰ range from +26.8 to +22.7‰, while results from the Elgin sample fall within a 2.7‰ range, from +22.4 to +19.7‰ (Fig. 10).

Seventy-nine $\delta^{18}O$ measurements were also made by ion microprobe on ten different overgrowths from two Wilcox sandstone samples from Lake Creek and Rotherwood Fields (Harwood, 2011). The $\delta^{18}O_{(qc)}$ of analysed overgrowths in the Wilcox samples show a 6.1‰ range from +24.7 to +18.6‰ for the Lake Creek sample, and a 5.5‰ range from +23.8 to +18.3‰ for the Rotherwood sample.

Analyses compromised by the occurrence of fluid inclusions or which fell within cracks or included detrital quartz were discarded. Apart from Elgin, where $\delta^{18}O_{(qc)}$ does not change across the overgrowths, $\delta^{18}O_{(qc)}$ values for all sandstones decrease from heavier values in the earliest formed cement to lighter values in latest formed cement (Fig. 10). Also, the $\delta^{18}O_{(qc)}$ versus distance plots (Fig. 10) do not show smooth trends from the detrital boundary to the edge of the overgrowth. These fluctuations, combined with the varied CL zoning in overgrowths (e.g. Fig. 8), demonstrates that the development of quartz cements is more complex than a simple concentric growth pattern.

4.3. Temperature-controlled quartz cementation models

Results of the quartz cementation modelling are shown in Fig. 11 and predict that, with the exception of Clyde, all the sandstones in this study have experienced sufficient levels of thermal stresses to be completely cemented with quartz. However, there is a very poor agreement between modelled and measured quartz cement volumes (Table 4). The respective 30 and 50% grain-coatings coverage estimated from petrographic analyses for the Fulmar Formation samples from Elgin and Clyde Fields were incorporated in the models. Zero grain-coatings coverage was used for the Wilcox Group sandstones from Rotherwood and Lake Creek Fields. The model overpredicts quartz cement volumes by 50 and 80% in sandstones from the high temperature Rotherwood and Elgin Fields respectively (Fig. 11 and Table 4). Similarly, the model overpredicts quartz cement volumes by 30 and 55% for the sandstones from Lake Creek and Clyde Fields respectively (Fig. 11 and Table 4).

5. Discussion

5.1. Quartz cementation histories

Since the oxygen isotope composition of a mineral is a dual function of temperature and $\delta^{18}O_{(water)}$ (Clayton et al., 1972), our $\delta^{18}O_{(qc)}$ data cannot alone provide a unique temperature history of quartz precipitation. The data can, however, be interpreted to make the most geologically realistic deductions if we make reasonable assumptions about the evolving oxygen isotope composition of the water from which the quartz precipitated. The framework for this is shown in Fig. 13 and is based on the quartz-water oxygen isotope fractionation factors reported by Matsuhisa et al. (1979).

Present-day $\delta^{18}O_{(water)}$ in Fulmar Formation sandstones in the

Table 3
Petrographic data of the studied Wilcox Group sandstones. All data from Harwood (2011), except Intergranular Pressure Dissolution (IPD) data. Bt = Berthierine, M/I = Mica/Illite, K–F = K-Feldspar, Na–F = Na-Feldspar, Ch = Chlorite, An = Ankerite.

Field	Sample size	Average quartz cement (%)	Average detrital quartz (%)	Quartz Cement/ Detrital Quartz	IPD (%)	IPD/Detrital Quartz	Non-quartz minerals (%)	Porosity (%)	Average grain size (mm)
Lake Creek	1	18.8	53.4	0.35	19.7	0.37	M/I, Bt, K–F (16%)	11.8	0.17
Rotherwood	1	12.3	56.9	0.22	11.7	0.21	Ch, M/I, Bt, Na–F, An (24%)	6.8	0.16

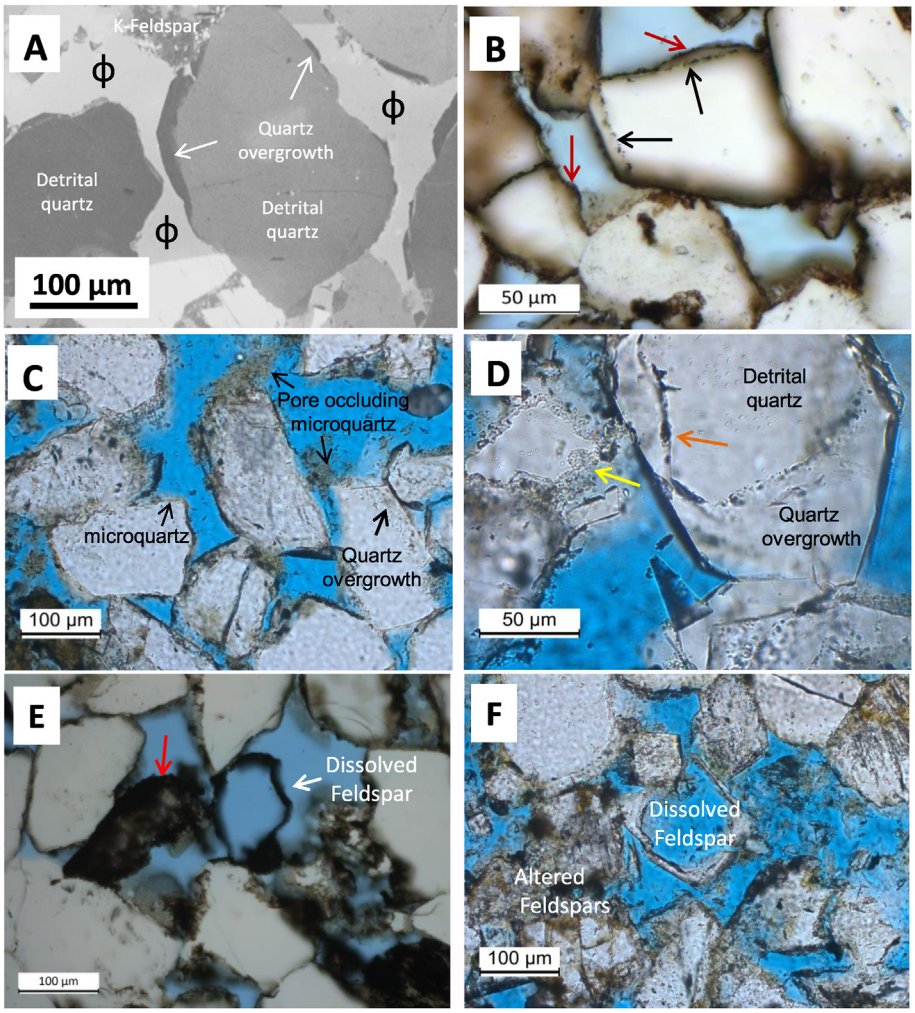

Fig. 7. A) Cathodoluminescence (CL) image of Fulmar Formation sample from Elgin Field showing partially dissolved feldspar, quartz cement and detrital quartz. Quartz overgrowths have stunted growth despite significant porosity and the very high present-day temperature (~190 °C). B) Optical thin-section photomicrograph (plane polarized) of Fulmar Formation sample from Elgin Field showing bitumen impregnated authigenic illite (red arrows) coating already precipitated macroquartz cement surfaces. Macroquartz cements completely engulfed grain-coating illite (black arrow). The blue areas represent porosity (Image from Fig. 6 in Oye et al., 2018). C) Optical thin-section photomicrograph (plane polarized) of Fulmar Formation from Clyde Field showing detrital grains with macroquartz and microquartz overgrowths. Pore-occluding microquartz cements are also present. D) Optical thin-section photomicrograph (plane polarized) of Fulmar Formation from Clyde field showing the coexistence of adjacent detrital grains completely enveloped by either microquartz or macroquartz overgrowths. The orange arrow points to poorly-developed clay coat on the detrital quartz with thick macroquartz overgrowth. The yellow arrow points at the well-developed grain-coating microquartz completely coating available surface area on the other detrital quartz grain. E) Optical thin-section photomicrograph (cross polarized) of Fulmar Formation from Elgin Field showing bitumen-impregnated clay rim preserving the shape of completely dissolved feldspar; the red arrow points at partially dissolved feldspar impregnated with bitumen. F) Optical thin-section photomicrograph (plane polarized) of Fulmar Formation from Clyde field showing altered feldspars, and preserved K-feldspar overgrowth outlining the shape of dissolved detrital K-feldspar. (For interpretation of the references to colour in this figure legend, the reader is referred to the Web version of this article.)

Clyde-Elgin area is around +4.5‰ (Hendry et al., 2000), and values more positive than this are unusual for Jurassic reservoirs in the Central North Sea (Warren et al., 1994). The first quartz cement to precipitate in Clyde sandstones has $\delta^{18}O_{(qc)}$ of +26.8‰, and the first to precipitate in Elgin has $\delta^{18}O_{(qc)}$ of +22.4‰. If precipitation began in waters similar to Jurassic seawater ($\delta^{18}O_{(water)}$ = −1‰), this represents 55 °C in Clyde and 80 °C in Elgin. Similarly, if the last quartz to form (+22.7‰ and +19.7‰ in Clyde and Elgin respectively) precipitated from water that had evolved to a value of +4.5‰ at present-day, this would correspond to temperatures of 125 °C in Clyde and 150 °C in Elgin (Fig. 13A). The temperature ranges for quartz cementation are then 55–125 °C in Clyde and 80–150 °C in Elgin.

A similar logic can be applied to the Wilcox Group sandstones. Here, Land and Fisher (1987) reported present-day $\delta^{18}O_{(water)}$ ranging from +3.5 to +5.8‰ measured over a wide range of temperature for Wilcox Group sandstones from fields adjacent to the study areas (Fig. 13B). If quartz precipitation started with $\delta^{18}O_{(qc)}$ of +24.7‰ in Lake Creek Field and +23.8‰ in Rotherwood Field from waters similar to Eocene seawater (−1‰), all quartz cementation could have occurred in $\delta^{18}O_{(water)}$ that evolved from −1 to +3.5‰ at the present-day. This would give a temperature window for quartz cementation of 65–145 °C in Lake Creek and 74–160 °C in Rotherwood Field (Fig. 13B). If $\delta^{18}O_{(water)}$ in Rotherwood Field is +5.8‰, then cementation occurs to maximum burial temperature. These data imply that quartz cementation occurred up to maximum burial temperature only in Lake Creek, and perhaps in Rotherwood Field.

It is rather surprising that cementation did not apparently continue to maximum burial temperature. A plausible explanation for is this that cementation did in fact continue up to maximum burial temperature but is not captured by the SIMS data, as it is very difficult to make analyses to the very edge of the quartz overgrowth (Fig. S4). In all cases, however, the amount of cement precipitating within 20–30 °C of the maximum temperatures would be small.

The inevitable uncertainties in the interpretation of $\delta^{18}O_{(qc)}$ data, in

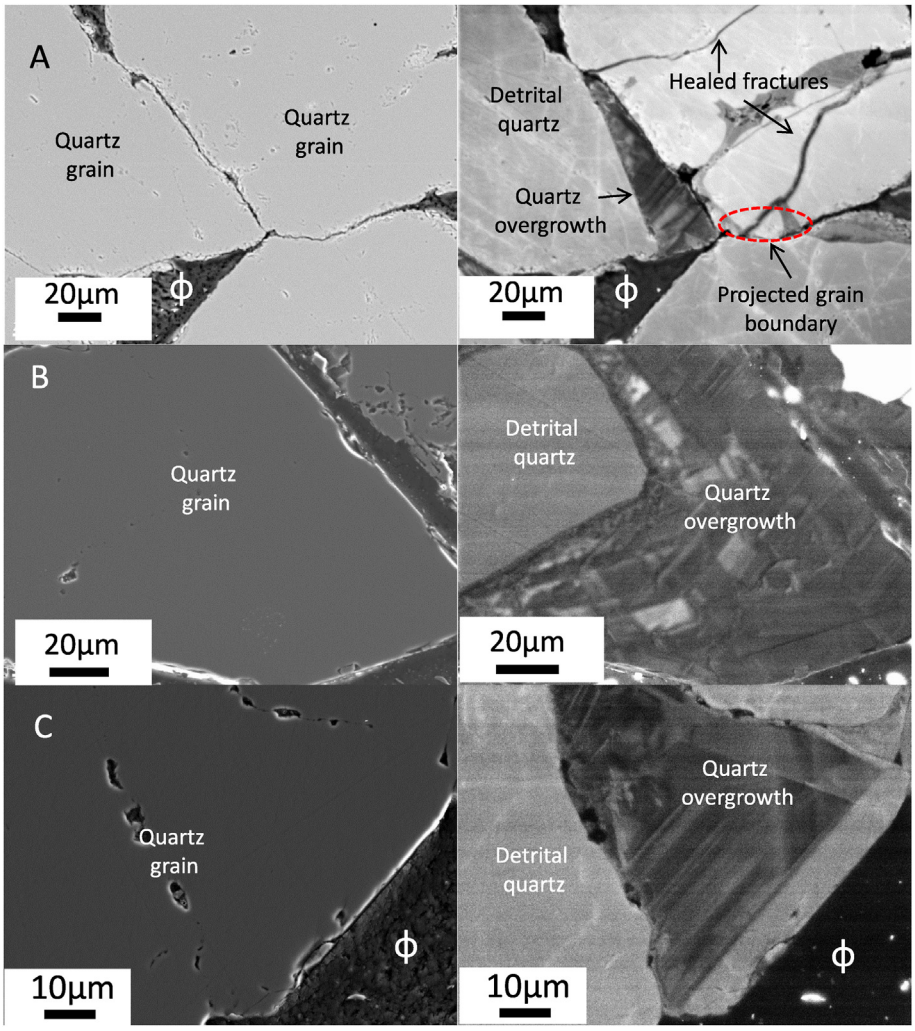

Fig. 8. Back-scattered electron (BSE) images (left) and equivalent cathodoluminescence (CL) images (right) of Upper Jurassic Fulmar sandstones showing A) sample projected grain boundary (after Sibley and Blatt (1976) and Houseknecht (1991)) used to define and quantify pressure dissolution, and healed grain fractures; B) quartz grain from Clyde sample set with very thick syntaxial overgrowth typified by mosaic-type CL zoning; C) quartz grain from Elgin sample set with syntaxial overgrowth showing angular CL zonation. These zoning patterns show that the idea of an overgrowth nucleating concentrically on detrital quartz, as assumed in quartz cementation model, is not always the case. Generally, overgrowth thicknesses are up to 60 µm in Elgin samples, and 100 µm in Clyde samples.

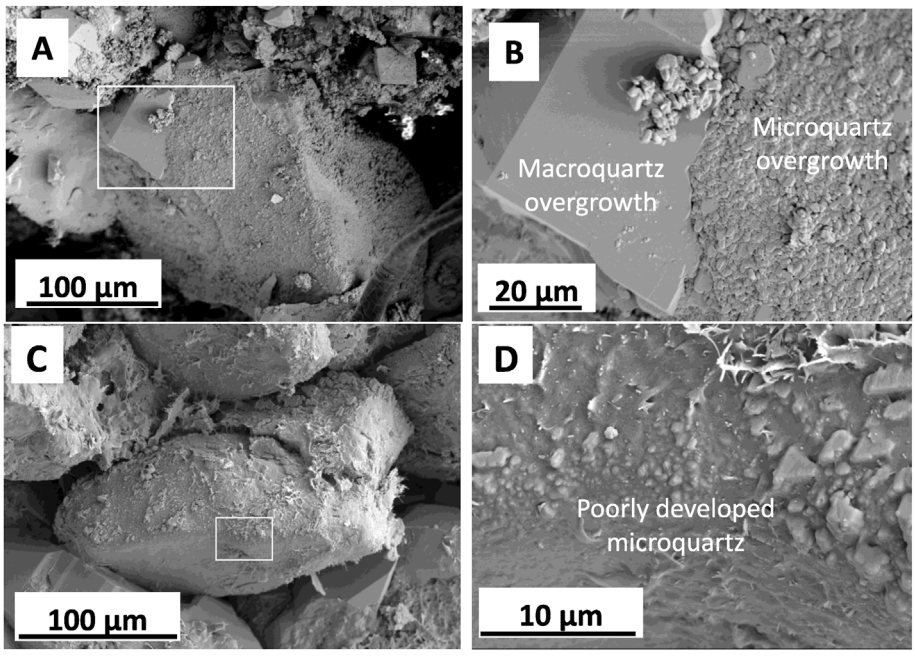

Fig. 9. Micrographs of Upper Jurassic Fulmar Formation sandstones from Clyde and Elgin Fields A) Scanning electron microscope (SEM) image of Clyde sample showing macroquartz and microquartz overgrowths nucleated on the same detrital quartz. B) Higher magnification view equivalent to the box in panel A. C) SEM image of Elgin sample showing quartz grain surface with poorly developed microquartz overgrowth and clay coats. D) Higher magnification of the box in panel C. Microquartz overgrowth are effectively absent in the Elgin samples (Images from Fig. 5 in Oye et al., 2018).

Table 4
Comparison of modelled and measured quartz cement volumes for sandstones from all the study locations.

	Clyde	Elgin	Rotherwood	Lake Creek
Temperature (°C)	147	189	185	143
Modelled Quartz Cement (%)	10.1	26.0	26.0	26.0
Measured Quartz Cement (%)	4.4	4.6	12.3	18.8

terms of the exact range of temperature and thus time over which cementation occurred, means that we cannot determine the precise rate of quartz cementation through the full burial history. In general, the fact that there is much more quartz cement in the younger Wilcox sandstones compared to the older Fulmar sandstones, indicates that cementation rates in the Wilcox sandstones were on average greater than those in the Fulmar sandstones. Similarly, if we assume that quartz cementation started at temperatures between 60 and 80 °C (Walderhaug, 1994a), the Fulmar sandstones have spent much longer in the proposed quartz cementation "window" than the Wilcox sandstones. Placing the $\delta^{18}O_{(qc)}$ data into the context of the time-temperature and time-vertical effective stress histories (Fig. 5) for each well support these qualitative statements and suggests that:

a) Quartz cementation rates are on average *slower* in lower vertical effective stress Fulmar Formation sandstones than higher vertical effective stress Wilcox Group sandstones.
b) Quartz cementation rates are on average *slower* in Fulmar Formation and Wilcox Group sandstones from the high temperature Elgin and Rotherwood Fields than their low temperature counterparts from Clyde and Lake Creek.

5.2. Silica supply and quartz cementation

Quantitative petrographic data show that local, intergranular pressure dissolution could have supplied between 95 and 115% of the silica required for quartz cementation in the studied Wilcox Group sandstones, and 60% of silica in the studied Fulmar Formation sandstones (Table 5). Fully- or partly-dissolved feldspars occur in both the Fulmar Formation and Wilcox Group sandstones (Fig. 6A and B, Fig. 7E and F) and provide an additional local source of silica via reactions such as the conversion of K-feldspar to illite:

$$1.0\ \text{K-feldspar} + 0.174H_2O + 0.522\ H^+ + 0.109\ Mg^{2+} = 0.739\ K^+ + 0.435\ \text{Illite} + 1.478\ \text{Quartz}$$

Oye et al. (2018) have shown that enough silica is released from this mid-late diagenetic reaction to account for the difference between the observed quartz cement and the silica supplied through intergranular pressure solution in Elgin. Although dissolved feldspar ghosts are less obvious in Clyde compared with Elgin, we suggest that the very common occurrence of oversized pores in Clyde indicates that the silica deficit can be filled in the same way. Fig. 12A also suggests that precipitation started around 50 °C; an indication that silica for early-formed quartz cement might have been sourced from seawater (Harwood et al., 2013). In summary, in all four cases, all or most of the silica requirement is fulfilled by local intergranular pressure dissolution, with the remainder in the Fulmar sands from local feldspar dissolution.

5.3. Does vertical effective stress exert an influence on quartz cementation?

Quantitative petrographic observations, inferred cementation histories, and modelled temperature and vertical effective stress histories combine to suggest that the history of vertical effective stress may exert an important influence on quartz cementation in these four studies. The key observations are:

1. Although some silica can be sourced from feldspar dissolution in the Fulmar, the majority of the silica required for the observed volumes of quartz cement can be supplied through local intergranular pressure dissolution, in all four case studies (Table 5). The amount and inferred rate of intergranular pressure dissolution is commonly considered to be controlled by vertical effective stress, with a secondary influence of temperature (De Boer et al., 1977; Dewers and Ortoleva, 1990, 1991; Elias and Hajash, 1992; Gratier et al., 2005; Nenna and Aydin, 2011; Oye et al., 2018; Renard et al., 1997; Robin, 1978; Rutter and Elliott, 1976; Sheldon et al., 2003; Shimizu, 1995;

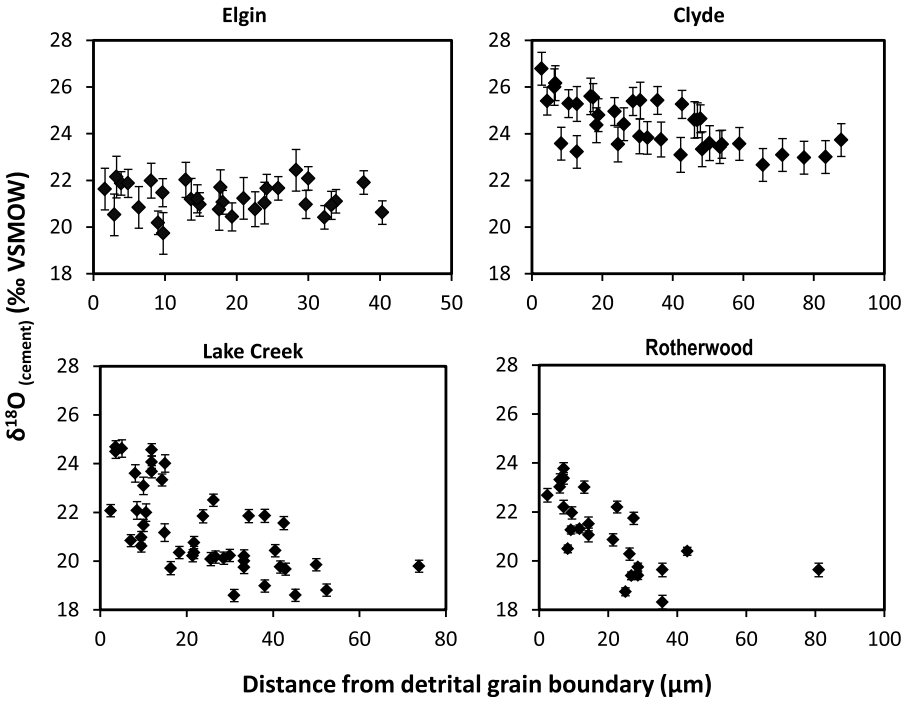

Fig. 10. Plot of $\delta^{18}O_{(quartz\ cement)}$ against distance in microns from detrital grain boundaries. Distance axis is limited to 50 µm in Elgin, 80 µm in Lake Creek, and 100 µm in Clyde and Rotherwood. Clyde and Elgin data were acquired from three overgrowths each using 3 µm SIMS spot sizes. Lake Creek and Rotherwood data were acquired from six and four overgrowths respectively using 12 µm SIMS spot sizes. All $\delta^{18}O_{(quartz\ cement)}$ decrease from heavier values close to detrital grain boundary to lighter values at the outermost edge of the overgrowths with the exception of Elgin samples.

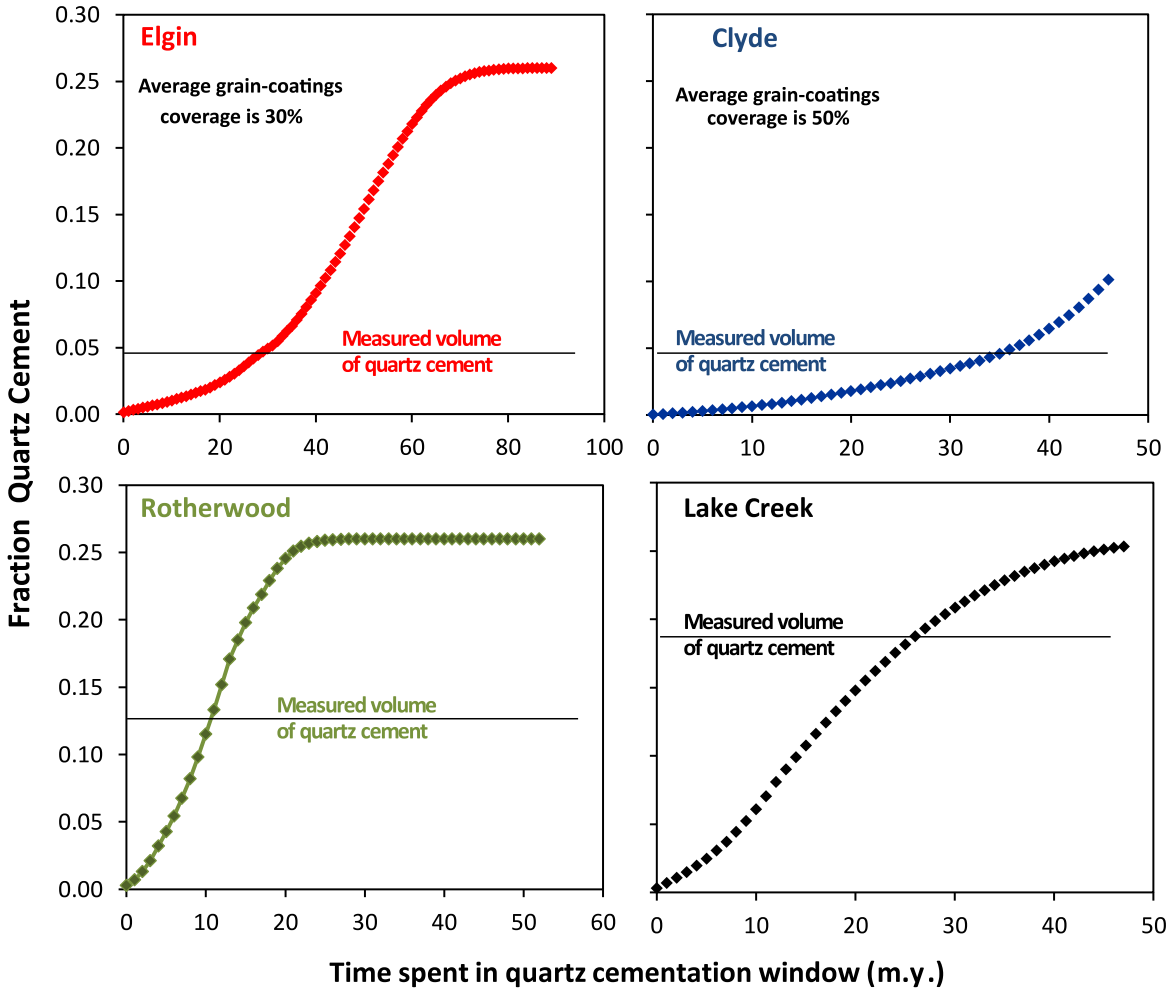

Fig. 11. Models showing quartz precipitation from quartz cementation threshold (80 °C) to present-day for Fulmar Formation from Elgin and Clyde Fields, and Wilcox Group sandstones from Rotherwood and Lake Creek Fields. Walderhaug (1996) approach was applied to 1 cm^3 volume of the studied sandstones using an 80 °C threshold temperature for cementation and a starting porosity of 26%. Time-temperature history was generated using PetroMod version 2014.1. Average grain-coatings coverage in Elgin and Clyde samples sets are approximately 30 and 50% respectively. Grain coatings in Clyde Field include both clays and microquartz. Grain coatings are very rare in the studied Wilcox Group sandstones.

Tada et al., 1987; Tada and Siever, 1989; van Noort et al., 2008; Weyl, 1959).

2. At a given temperature, the amount of quartz cement is much lower in the sandstones that have experienced lower vertical effective stress through their history (Lake Creek versus Clyde; Rotherwood versus Elgin; Fig. 5). In addition, both the Wilcox and Fulmar sandstones buried to higher temperatures and greater thermal stress, Rotherwood and Elgin, have less quartz cement than their lower temperature counterparts (Fig. 11; Table 5).
3. Measured volumes of quartz cement are lower than those predicted by temperature-controlled precipitation models for all the studied sandstones (Figs. 11 and 13B), especially for the sandstones that have never experienced high vertical effective stress. Although it would be possible to obtain local calibrations to quartz cement volumes by altering the kinetic constants in either the Walderhaug (1996) or Arrhenius-based (Lander et al., 2008; Taylor et al., 2015; Walderhaug, 2000) quartz cementation models, very different values would be needed for Wilcox and for Fulmar. We suggest that the need for different kinetic constants implies that quartz cementation must be influenced by factors other than the temperature-controlled rate of quartz precipitation (Ajdukiewicz and Lander, 2010; Lander et al., 2008; Walderhaug, 1994a, 1996, 2000).

Table 5
Normalised quartz cement contents for the Fulmar Formation and Wilcox Group sandstones. VES = Vertical Effective Stress; $\delta^{18}O_{(qc)}$ is the oxygen isotope composition of quartz cement. VES in Clyde is the proposed VES 0.5 Ma ago, prior to reduction in pore pressure as a result of lateral fluid drainage (Swarbrick et al., 2005). Present-day VES in Clyde is 40 MPa. Temp. Range is the temperature range over which quartz cement is suggested to form, based on oxygen isotope composition. IPD is intergranular pressure dissolution.

Field	Modelled Quartz Cement (%)	Measured Quartz Cement (%)	Quartz Cement/Detrital Quartz	IPD/Detrital Quartz	Temp. (°C)	VES (MPa)	$\delta^{18}O_{(qc)}$ range	Temp. Range (°C)
Elgin	26.0	4.6	0.12	0.07	189	12.5	2.7	80–150
Clyde	10.1	4.4	0.15	0.09	147	19.2	4.1	55–125
Rotherwood	26.0	12.3	0.22	0.21	185	23.2	5.5	75–160
Lake Creek	26.0	18.8	0.35	0.37	143	33.7	6.1	65–145

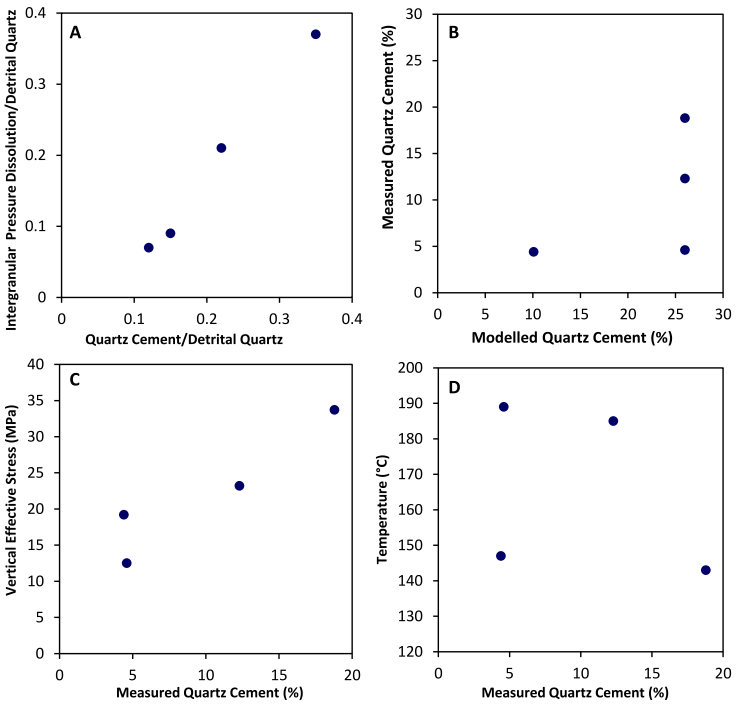

Fig. 12. (A) Intergranular pressure dissolution versus quartz cement. All data have been normalised to detrital quartz content to avoid bias that may result from variations in the detrital mineralogical composition of the samples (see Houseknecht, 1984; Houseknecht, 1988; Houseknecht, 1991). (B) Measured quartz cement against modelled quartz cement from Walderhaug (1996) model. Note the low volumes of measured quartz cement compared to modelled quartz cement. (C) Present-day vertical effective stress versus measured quartz cement. (D) Present-day temperature versus measured quartz cement. Each point represents data from a single field. See Table 5 for data plotted in this figure.

We interpret these observations to suggest that the vertical effective stress-controlled supply of silica from intergranular pressure dissolution exerts an important influence on quartz cementation. This has been suggested previously (Elias and Hajash, 1992; Osborne and Swarbrick, 1999; Oye et al., 2018; Sheldon et al., 2003; van Noort et al., 2008), but the idea may not have gathered support, perhaps because it can be difficult to unravel the relative effects of time-temperature and time-vertical effective stress histories. Accepting that it is difficult to obtain accurate histories of vertical effective stress from basin models, it is not uncommon to observe a general positive relationship between temperature and vertical effective stress during burial. As an illustration, if pore pressure remains hydrostatic throughout the burial history of a sandstone, there will be a very strong correlation between increasing temperature and increasing effective stress through the sediment's burial history. It is only by studying samples from sandstones with very different histories of vertical effective stress, such as those described here, that the relative influence of temperature and stress can be examined.

Although beyond the scope of this paper, a critical predictive next step would be to quantify the rate of intergranular pressure dissolution as a dual function of vertical effective stress and temperature. A paper by van Noort et al. (2008) presents such a model, based on higher temperature laboratory experiments, but it has never been tested against data in sandstones in sedimentary basins. Some initial insights can be gleaned from the current study, in that vertical effective stress in Clyde Field has increased from 19 to 40 MPa in the last 0.5 million years but has quartz cement volumes which are qualitatively consistent with the lower vertical effective stress value. This suggests that the kinetics of intergranular pressure dissolution are geologically slow, such that greater (sub million-year) timescales are required for the results of intergranular pressure dissolution to be observed as quartz cement.

5.4. Can the pattern of quartz cementation be explained by other factors?

The occurrences of grain-coating clays and microquartz, and the emplacement of petroleum into sandstone reservoirs, have been extensively discussed as ways in which macroquartz cementation can be inhibited. We now discuss - and dismiss - these mechanisms as important controls on quartz cementation in these sandstones.

Pervasive grain-coating clays and microquartz are very effective inhibitors of quartz cementation (Ajdukiewicz and Lander, 2010; Berger et al., 2009; Dutton et al., 2016; Morad et al., 2010; Nguyen et al., 2013; Stricker et al., 2016; Taylor et al., 2010, 2015) but cannot account for the low amounts of cement in these sandstones. In the Wilcox sandstones, microquartz was not observed and some of the minute grain-coating clays present have been engulfed by quartz cement. Grain-coating microquartz was observed in variable abundance in the Clyde sample set. Although samples with the most grain-coating microquartz overgrowths have the least quartz cement, quantitative CL petrography revealed that other samples with little or no microquartz have very low volumes of quartz cement compared to the volume predicted by the temperature-dependent quartz cementation model (Fig. 11 and Table 3). Grain-coating microquartz is very rare in sandstones from Elgin and thus has no effect on quartz cementation.

The Fulmar Formation sandstones in this study are upper shoreface facies with low volumes of illitic clays (< 3%). The detrital or authigenic origin of these clays is not easily discernible as detrital illite can recrystallise as a function of temperature (Wilkinson and Haszeldine, 2011). Grain-coating illite derived from feldspar alteration is unlikely to have inhibited quartz cementation, because quartz cement would have precipitated on free detrital quartz surfaces prior to feldspar dissolution (Oye et al., 2018). Petrographic evidence (Fig. 7) confirms this assertion, as authigenic illite coating the surfaces of some macroquartz overgrowths suggests that macroquartz cementation predates authigenic illite formation. Illite of detrital origin forms early on detrital grains and is likely to possess more inhibitive effect on quartz cementation. However, petrographic observation of the Fulmar Formation sandstones shows that poorly-developed grain coatings have been completely engulfed by quartz cement (Fig. 7).

Quantitative analysis shows that the combined average grain-coat coverage of clay and microquartz is less than 50% in the Fulmar Formation samples from Clyde and Elgin Fields (Fig. 14). Quartz cementation modelling performed on the Fulmar Formation sandstones were tested with varying grain-coat coverage values. The outputs suggest that each detrital quartz grain requires grain-coat coverage of

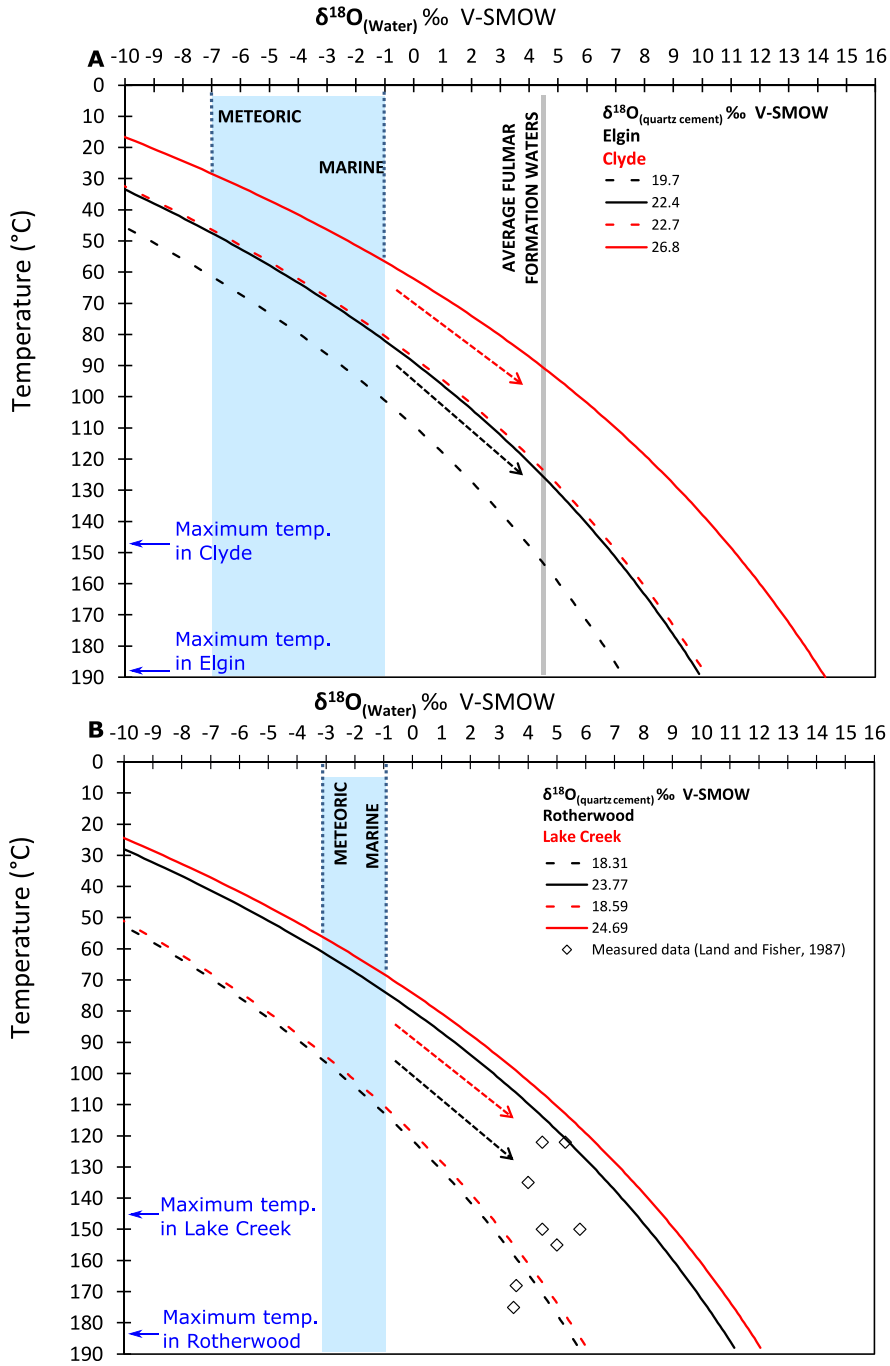

Fig. 13. Plot showing $\delta^{18}O_{(water)}$ in equilibrium with $\delta^{18}O_{(quartz\ cement)}$ as a function of temperature (Matsuhisa et al., 1979). (A) Red and black $\delta^{18}O_{(quartz\ cement)}$ Vienna Standard Mean Ocean Water (VSMOW) contours represent the $\delta^{18}O$ range from early to late quartz cement in Clyde and Elgin. $\delta^{18}O_{(water)}$ likely evolved from Jurassic marine water to present-day formation water (~4.5‰) in the Fulmar reservoirs in Clyde and Elgin fields. (B) Red and black $\delta^{18}O_{(quartz\ cement)}$ VSMOW contours represent $\delta^{18}O$ range from early to late quartz cement in Lake Creek and Rotherwood Fields. $\delta^{18}O_{(water)}$ likely evolved from Tertiary marine water to present-day formation water (+3.5 to + 5.8‰) in Lake Creek and in Rotherwood. These $\delta^{18}O_{(water)}$ are based on measured data from Wilcox Group sandstones from adjacent fields in the onshore Gulf Coast region (Land and Fisher, 1987). Evolution paths in graphs A and B are depicted by red (Clyde and Lake Creek) and black (Elgin and Rotherwood) arrows. (For interpretation of the references to colour in this figure legend, the reader is referred to the Web version of this article.)

around 80% in Clyde Field, and 99% in Elgin Field, to limit the observed average quartz cement volumes in both fields to their current values (4.4 and 4.6%). The required coating coverage is thus much higher than those observed.

The possible role of hydrocarbon emplacement as an inhibitor of quartz cementation in sandstone reservoirs has been discussed in many studies (e.g. Aase et al., 1996; Aase and Walderhaug, 2005; Dixon et al., 1989; Emery et al., 1993; Gluyas et al., 1993; Marchand et al., 2000; Marchand et al., 2002; Molenaar et al., 2008; Saigal et al., 1992; Wilkinson and Haszeldine, 2011; Worden et al., 2018a; Worden et al., 2018b; Worden et al., 1998). In this study, basin modelling suggests that all the studied sandstones were charged with hydrocarbons from the Miocene, except for the Elgin reservoir that was charged from the Eocene. These timings are similar to those estimated in previous studies of the Fulmar Formation and Wilcox Group sandstones (see Pitman and Rowan, 2012; Rudkiewicz et al., 2000; Stevens and Wallis, 1991). Comparison of the charge histories with modelled and actual cementation histories estimated from oxygen isotope data, indicate that the effect of hydrocarbon emplacement on quartz cementation in the studied sandstones is negligible. Firstly, temperature-based quartz precipitation models predict that substantial quartz cement should have precipitated prior to hydrocarbon emplacement and secondly, quartz cementation histories from *in situ* oxygen isotope analysis suggest that cementation continued beyond the time of hydrocarbon emplacement, potentially to the present-day. These results show no evidence that hydrocarbon emplacement has played a significant role on quartz cementation in the studied sandstones.

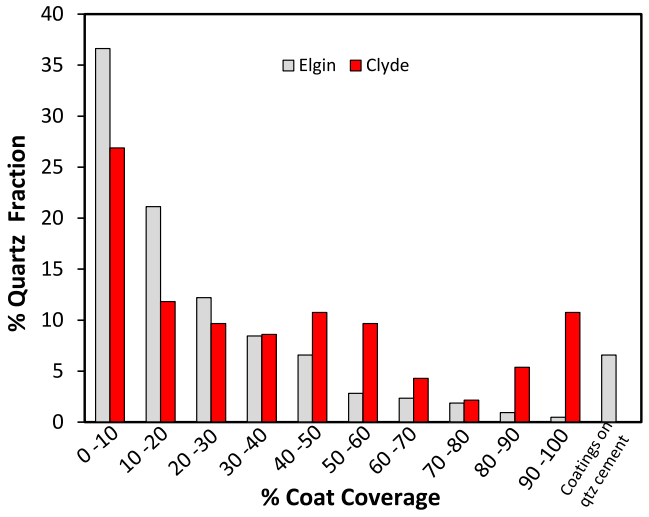

Fig. 14. Percentage of detrital quartz fraction in the analysed Upper Jurassic Fulmar Formation sandstones from Clyde and Elgin Fields, and their corresponding percentage grain coat coverage. Average grain coat coverage in both Clyde and Elgin Field is less than 40%. The analysed grain coatings in Clyde include clays and microquartz.

6. Summary and conclusions

We have presented quantitative petrographic data, high spatial resolution oxygen isotope analyses of quartz cement, basin modelling and a kinetic model for quartz precipitation for two Paleocene-Eocene Wilcox Group sandstones from Texas and two Jurassic Fulmar Formation sandstones from the Central North Sea. In each basin, one sandstone has been buried to *ca.* 145 °C and one to *ca.* 185 °C.

The amounts of quartz cement in the Wilcox sandstones are between 12 and 18%, and between 2 and 6% in the Fulmar sandstones. Oxygen isotope data suggest that in all cases, quartz cementation occurred from 60 to 80 °C to temperatures close to maximum burial. Petrographic data show that most of the silica for quartz cement can be derived from intergranular pressure dissolution, with an additional contribution in Fulmar sandstones from feldspar alteration. There is no strong evidence that factors such as grain coatings or the timing of petroleum emplacement can explain the differences in the amounts of quartz cement in these Wilcox and Fulmar samples.

A key difference between the Wilcox and Fulmar sandstones is their history of vertical effective stress. The Wilcox sandstones in this study are currently at much higher vertical effective stresses than the Fulmar sandstones, and basin modelling studies suggest that they have been subjected to generally higher vertical effective stresses through their burial history. Both the extent of intergranular pressure dissolution and of quartz cementation are more strongly related to vertical effective stress than to temperature. We therefore suggest that the differences in quartz cementation in Fulmar and Wilcox sandstones can be explained better by differences in their vertical effective stress history than their temperature history. In this case, the rate of intergranular pressure solution would be an important control on quartz cementation, and an important next step would be to quantify the rate of intergranular pressure dissolution as a function of both vertical effective stress and temperature. In the Clyde case study presented here, vertical effective stress has increased from 19 to 40 MPa in the last 0.5 million years but sandstones have quartz cement volumes which are qualitatively consistent with the lower vertical effective stress value. This suggests that the kinetics of intergranular pressure dissolution are slow on a sub million-year timescale.

Because it is not uncommon for both temperature and vertical effective stress to increase as sedimentary rocks are buried, it can be difficult to unravel the relative importance of temperature and vertical effective stress histories as potential controls on quartz cementation. From a petroleum exploration perspective, the limited datasets presented here suggest that sandstones which have been buried to high temperature, but which have been subjected to a history of low effective stress, could still be effective reservoirs.

CRediT authorship contribution statement

Olakunle J. Oye: Writing - original draft, Writing - review & editing, Conceptualization, Data curation, Methodology, Project administration, Investigation, Software, Resources, Validation, Visualization, Formal analysis, Funding acquisition. **Andrew C. Aplin:** Writing - original draft, Writing - review & editing, Conceptualization, Supervision. **Stuart J. Jones:** Writing - review & editing, Conceptualization, Supervision. **Jon G. Gluyas:** Writing - review & editing, Conceptualization, Supervision. **Leon Bowen:** Formal analysis. **Joseph Harwood:** Formal analysis. **Ian J. Orland:** Writing - review & editing, Formal analysis. **John W. Valley:** Writing - review & editing, Funding acquisition.

Acknowledgments

Petroleum Technology Development Fund, Nigeria is thanked for funding this research. We acknowledge support from the British Geological Survey (BGS) for access to core material, and Information Handling Services (IHS) for access to data from Central North Sea wells. Core samples of Wilcox sandstones were provided to Joseph Harwood by the Bureau of Economic Geology, The University of Texas at Austin. Some of those samples were used in this study. WiscSIMS is supported by the U.S. National Science Foundation (EAR-1658823) and the University of Wisconsin- Madison. JWV is supported by the U.S. Department of Energy, Office of Basic Energy Sciences, Geosciences under Award Number DE-FG02-93ER14389. We thank anonymous reviewers for their constructive comments on the original manuscript.

Appendix A. Supplementary data

Supplementary data to this article can be found online at https://doi.org/10.1016/j.marpetgeo.2020.104289.

References

Aase, N.E., Bjorkum, P.A., Nadeau, P.H., 1996. The effect of grain-coating microquartz on preservation of reservoir porosity. AAPG Bull. 80, 1654–1673.
Aase, N.E., Walderhaug, O., 2005. The effect of hydrocarbons on quartz cementation: diagenesis in the Upper Jurassic sandstones of the Miller Field, North Sea, revisited. Petrol. Geosci. 11, 215–223.
Ajdukiewicz, J., Nicholson, P., Esch, W., 2010. Prediction of deep reservoir quality using early diagenetic process models in the Jurassic Norphlet Formation, Gulf of Mexico. AAPG Bull. 94, 1189–1227.
Ajdukiewicz, J.M., Lander, R.H., 2010. Sandstone reservoir quality prediction: the state of the art. AAPG Bull. 94, 1083–1091.
Allen, P., Allen, J., 1990. Basin Analysis–Principles and Applications, first ed. Blackwell Scientific Publications, Oxford, pp. 449.
Berger, A., Gier, S., Krois, P., 2009. Porosity-preserving chlorite cements in shallow-marine volcaniclastic sandstones: evidence from Cretaceous sandstones of the Sawan gas field, Pakistan. AAPG Bull. 93, 595–615.
Bjorkum, P.A., 1996. How important is pressure in causing dissolution of quartz in sandstones? J. Sediment. Res. 66, 147–154.
Bjorlykke, K., Egeberg, P., 1993. Quartz cementation in sedimentary basins. AAPG Bull. 77, 1538–1548.
Bloch, S., Lander, R.H., Bonnell, L., 2002. Anomalously high porosity and permeability in deeply buried sandstone reservoirs: origin and predictability. AAPG Bull. 86, 301–328.
Clayton, R.N., O'Neil, J.R., Mayeda, T.K., 1972. Oxygen isotope exchange between quartz and water. J. Geophys. Res. 77, 3057–3067.
Day-Stirrat, R.J., Milliken, K.L., Dutton, S.P., Loucks, R.G., Hillier, S., Aplin, A.C., Schleicher, A.M., 2010. Open-system chemical behavior in deep Wilcox Group mudstones, Texas Gulf Coast, USA. Mar. Petrol. Geol. 27, 1804–1818.
De Boer, R., Nagtegaal, P., Duyvis, E., 1977. Pressure solution experiments on quartz sand. Geochem. Cosmochim. Acta 41, 257–264.
Denny, A.C., Fall, A., Orland, I.J., Valley, J.W., Eichhubl, P., Laubach, S., 2019. A prolonged history of pore water oxygen isotope evolution in the cretaceous Travis peak

formation in East Texas. Geol. Soc. Am. Bull. 0, 1–13. https://doi.org/10.1130/B35291.1.
Dewers, T., Ortoleva, P., 1990. A coupled reaction/transport/mechanical model for intergranular pressure solution, stylolites, and differential compaction and cementation in clean sandstones. Geochem. Cosmochim. Acta 54, 1609–1625.
Dewers, T., Ortoleva, P., 1991. Influences of clay minerals on sandstone cementation and pressure solution. Geology 19, 1045–1048.
Dixon, S., Summers, D., Surdam, R., 1989. Diagenesis and preservation of porosity in norphlet formation (upper jurassic), southern Alabama. AAPG (Am. Assoc. Pet. Geol.) Bull. 73, 707–728.
Dutton, S.P., Ambrose, W.A., Loucks, R.G., 2016. Diagenetic controls on reservoir quality in deep upper Wilcox sandstones of the rio grande delta system, south Texas. Gulf Coast Assoc. Geol. Soc. 5, 95–110.
Dutton, S.P., Loucks, R.G., 2010. Diagenetic controls on evolution of porosity and permeability in lower Tertiary Wilcox sandstones from shallow to ultradeep (200–6700m) burial, Gulf of Mexico Basin, USA. Mar. Petrol. Geol. 27, 69–81.
Elias, B.P., Hajash, A., 1992. Changes in quartz solubility and porosity due to effective stress: an experimental investigation of pressure solution. Geology 20, 451–454.
Emery, D., Smalley, P., Oxtoby, N., Ragnarsdottir, K., Aagaard, P., Halliday, A., Coleman, M., Petrovich, R., 1993. Synchronous oil migration and cementation in sandstone reservoirs demonstrated by quantitative description of diagenesis. Phil. Trans. Roy. Soc. Lond.: Math. Phys. Eng. Sci. 344, 115–125.
Fisher, R.S., Land, L.S., 1986. Diagenetic history of Eocene Wilcox sandstones, south-central Texas. Geochem. Cosmochim. Acta 50, 551–561.
Fisher, W.L., McGowen, J., 1967. Depositional Systems in the Wilcox group of Texas and their relationship to occurrence of oil and gas. Gulf Coast Assoc. Geol. Soc. Trans. 17, 105–125.
French, M.W., Worden, R.H., 2013. Orientation of microcrystalline quartz in the Fontainebleau Formation, Paris Basin and why it preserves porosity. Sediment. Geol. 284, 149–158.
French, M.W., Worden, R.H., Mariani, E., Larese, R.E., Mueller, R.R., Kliewer, C.E., 2012. Microcrystalline quartz generation and the preservation of porosity in sandstones: evidence from the upper cretaceous of the subhercynian basin, Germany. J. Sediment. Res. 82, 422–434.
Galloway, W.E., Ganey-Curry, P.E., Li, X., Buffler, R.T., 2000. Cenozoic depositional history of the Gulf of Mexico basin. AAPG Bull. 84, 1743–1774.
Gilham, R., Hercus, C., Evans, A., De Haas, W., 2005. Shearwater (UK Block 22/30b): managing changing uncertainties through field life. In: Geological Society, London, Petroleum Geology Conference Series. Geological Society of London, pp. 663–673.
Gluyas, J., Robinson, A., Emery, D., Grant, S., Oxtoby, N., 1993. The link between petroleum emplacement and sandstone cementation. In: Geological Society, London, Petroleum Geology Conference Series. Geological Society of London, pp. 1395–1402.
Gowland, S., 1996. Facies Characteristics and Depositional Models of Highly Bioturbated Shallow Marine Siliciclastic Strata: an Example from the Fulmar Formation (Late Jurassic). vol. 114. Geological Society, London, Special Publications, UK Central Graben, pp. 185–214.
Graham, C., Armour, A., Bathurst, P., Evans, D., Petroleumsforening, N., 2003. The millennium atlas: petroleum geology of the central and northern North Sea. Geol. Soc. Lond. 27 (49), 157–173.
Gratier, J.-P., Muquet, L., Hassani, R., Renard, F., 2005. Experimental microstylolites in quartz and modeled application to natural stylolitic structures. J. Struct. Geol. 27, 89–100.
Grigsby, J.D., Vidal, J.M., Luffel, D.L., Hawkins, J., Mendenhall, J.M., 1992. Effects of fibrous illite on permeability measurements from preserved cores obtained in lower Wilcox Group gas sandstones, Lake Creek Field, Montgomery County, Texas. Gulf Coast Assoc. Geol. Soc. Trans. 42, 161–172.
Harwood, J., 2011. The origin and timing of quartz cementation in reservoir sandstones: evidence from in-situ microanalysis of oxygen isotopes. Geosciences 310 Newcastle University, Newcastle University.
Harwood, J., Aplin, A.C., Fialips, C.I., Iliffe, J.E., Kozdon, R., Ushikubo, T., Valley, J.W., 2013. Quartz cementation history of sandstones revealed by high-resolution sims oxygen isotope analysis. J. Sediment. Res. 83, 522–530.
Heald, M., Larese, R., 1974. Influence of coatings on quartz cementation. J. Sediment. Res. 44, 1269–1274.
Hendry, J.P., Wilkinson, M., Fallick, A.E., Haszeldine, R.S., 2000. Ankerite cementation in deeply buried Jurassic sandstone reservoirs of the central North Sea. J. Sediment. Res. 70, 227–239.
Houseknecht, D.W., 1984. Influence of grain size and temperature on intergranular pressure solution, quartz cementation, and porosity in a quartzose sandstone. J. Sediment. Res. 54, 348–361.
Houseknecht, D.W., 1988. Intergranular pressure solution in four quartzose sandstones. J. Sediment. Res. 58, 228–246.
Houseknecht, D.W., 1991. Use of Cathodoluminescence Petrography for Understanding Compaction, Quartz Cementation, and Porosity in Sandstones. SEPM Special Publication SC25, pp. 59–66.
Kelly, J.L., Fu, B., Kita, N.T., Valley, J.W., 2007. Optically continuous silcrete quartz cements of the St. Peter Sandstone: high precision oxygen isotope analysis by ion microprobe. Geochem. Cosmochim. Acta 71, 3812–3832.
Kita, N.T., Ushikubo, T., Fu, B., Valley, J.W., 2009. High precision SIMS oxygen isotope analysis and the effect of sample topography. Chem. Geol. 264, 43–57.
Kuhn, O., Smith, S., Van Noort, K., Loiseau, B., 2003. 30/11b, UK North Sea. The Fulmar Field, Blocks 30/16, vol. 20. Geological Society, London, Memoirs, pp. 563–585.
Land, L.S., Fisher, R.S., 1987. Wilcox sandstone diagenesis, Texas Gulf Coast: a regional isotopic comparison with the Frio Formation. Geol. Soc. Lond. Spec. Publ. 36, 219–235.
Lander, R.H., Larese, R.E., Bonnell, L.M., 2008. Toward more accurate quartz cement models: the importance of euhedral versus noneuhedral growth rates. AAPG (Am. Assoc. Pet. Geol.) Bull. 92, 1537–1563.
Lander, R.H., Walderhaug, O., 1999. Predicting porosity through simulating sandstone compaction and quartz cementation. AAPG Bull. 83, 433–449.
Lasocki, J., Guemene, J., Hedayati, A., Legorjus, C., Page, W., 1999. The Elgin and Franklin Fields: UK Blocks 22/30c, 22/30b and 29/5b, Geological Society, London, Petroleum Geology Conference Series. Geological Society of London, pp. 1007–1020.
Maast, T.E., Jahren, J., Bjorlykke, K., 2011. Diagenetic controls on reservoir quality in Middle to upper jurassic sandstones in the south viking graben, North Sea. AAPG Bull. 95, 1937–1958.
Marchand, A., Haszeldine, R., Macaulay, C., Swennen, R., Fallick, A., 2000. Quartz cementation inhibited by crestal oil charge: miller deep water sandstone, UK North Sea. Clay Miner. 35 201-201.
Marchand, A.M., Haszeldine, R.S., Smalley, P.C., Macaulay, C.I., Fallick, A.E., 2001. Evidence for reduced quartz-cementation rates in oil-filled sandstones. Geology 29, 915–918.
Marchand, A.M., Smalley, P.C., Haszeldine, R.S., Fallick, A.E., 2002. Note on the importance of hydrocarbon fill for reservoir quality prediction in sandstones. AAPG Bull. 86, 1561–1572.
Matsuhisa, Y., Goldsmith, J.R., Clayton, R.N., 1979. Oxygen isotopic fractionation in the system quartz-albite-anorthite-water. Geochem. Cosmochim. Acta 43, 1131–1140.
McBride, E., Diggs, T., Wilson, J., 1991. Compaction of Wilcox and carrizo sandstones (Paleocene-Eocene) to 4420 M, Texas Gulf coast. J. Sediment. Res. 61 93 - 85.
McBride, E.F., 1989. Quartz cement in sandstones: a review. Earth Sci. Rev. 26, 69–112.
Molenaar, N., Cyziene, J., Sliaupa, S., Craven, J., 2008. Lack of inhibiting effect of oil emplacement on quartz cementation: evidence from Cambrian reservoir sandstones, Paleozoic Baltic Basin. Geol. Soc. Am. Bull. 120, 1280–1295.
Morad, S., Al-Ramadan, K., Ketzer, J.M., De Ros, L., 2010. The impact of diagenesis on the heterogeneity of sandstone reservoirs: a review of the role of depositional facies and sequence stratigraphy. AAPG Bull. 94, 1267–1309.
Nenna, F., Aydin, A., 2011. The formation and growth of pressure solution seams in clastic rocks: a field and analytical study. J. Struct. Geol. 33, 633–643.
Nguyen, B.T., Jones, S.J., Goulty, N.R., Middleton, A.J., Grant, N., Ferguson, A., Bowen, L., 2013. The role of fluid pressure and diagenetic cements for porosity preservation in Triassic fluvial reservoirs of the Central Graben, North Sea. AAPG Bull. 97, 1273–1302.
Nunn, J.A., Sassen, R., 1986. The framework of hydrocarbon generation and migration, Gulf of Mexico continental slope. Gulf Coast Assoc. Geol. Soc. Trans. 36, 257–262.
Osborne, M.J., Swarbrick, R.E., 1999. Diagenesis in North Sea HPHT clastic reservoirs—consequences for porosity and overpressure prediction. Mar. Petrol. Geol. 16, 337–353.
Oye, O.J., 2019. Influence of Fluid Pressure and Effective Stress on Quartz Cementation in ClasticReservoirs. Doctoral Thesis. pp. 12–22. Durham University. http://etheses.dur.ac.uk/13057.
Oye, O.J., Aplin, A.C., Jones, S.J., Gluyas, J.G., Bowen, L., Orland, I.J., Valley, J.W., 2018. Vertical effective stress as a control on quartz cementation in sandstones. Mar. Petrol. Geol. 98, 640–652.
Page, F., Ushikubo, T., Kita, N.T., Riciputi, L., Valley, J.W., 2007. High-precision oxygen isotope analysis of picogram samples reveals 2 μm gradients and slow diffusion in zircon. Am. Mineral. 92, 1772–1775.
Pitman, J.K., Rowan, E.R., 2012. Temperature and Petroleum Generation History of the Wilcox Formation, Louisiana, Open-File Report. US Geological Survey, Reston, VA, pp. i–51.
Pittman, E.D., 1972. Diagenesis of quartz in sandstones as revealed by scanning electron microscopy. J. Sediment. Res. 42, 507–519.
Pollington, A.D., Kozdon, R., Valley, J.W., 2011. Evolution of quartz cementation during burial of the cambrian mount simon sandstone, Illinois basin: in situ microanalysis of δ18O. Geology 39, 1119–1122.
Renard, F., Ortoleva, P., Gratier, J.P., 1997. Pressure solution in sandstones: influence of clays and dependence on temperature and stress. Tectonophysics 280, 257–266.
Robin, P.-Y.F., 1978. Pressure solution at grain-to-grain contacts. Geochem. Cosmochim. Acta 42, 1383–1389.
Robinson, A., Gluyas, J., 1992. Model calculations of loss of porosity in sandstones as a result of compaction and quartz cementation. Mar. Petrol. Geol. 9, 319–323.
Rudkiewicz, J., Penteado, H.d.B., Vear, A., Vandenbroucke, M., Brigaud, F., Wendebourg, J., Duppenbecker, S., 2000. Integrated basin modeling helps to decipher petroleum Systems. Petrol. Sys. South Atl. margins Mem. 73, 27–40.
Rutter, E., Elliott, D., 1976. The kinetics of rock deformation by pressure solution. Phil. Trans. Roy. Soc. Lond.: Math. Phys. Eng. Sci. 283, 203–219.
Saigal, G.C., Bjorlykke, K., Larter, S., 1992. The effects of oil emplacement on diagenetic processes: examples from the fulmar reservoir sandstones, Central North Sea: geologic note (1). AAPG (Am. Assoc. Pet. Geol.) Bull. 76, 1024–1033.
Sathar, S., Worden, R.H., Faulkner, D.R., Smalley, P.C., 2012. The effect of oil saturation on the mechanism of compaction in granular materials: higher oil saturations lead to more grain fracturing and less pressure solution. J. Sediment. Res. 82, 571–584.
Sheldon, H.A., Wheeler, J., Worden, R.H., Cheadle, M.J., 2003. An analysis of the roles of stress, temperature, and pH in chemical compaction of sandstones. J. Sediment. Res. 73, 64–71.
Shimizu, I., 1995. Kinetics of pressure solution creep in quartz: theoretical considerations. Tectonophysics 245, 121–134.
Sibley, D.F., Blatt, H., 1976. Intergranular pressure solution and cementation of the Tuscarora orthoquartzite. J. Sediment. Res. 46, 881–896.
Smith, D.L., Dees, W.T., Harrelson, D.W., 1981. Geothermal conditions and their implications for basement tectonics in the Gulf Coast margin. Gulf Coast Assoc. Geol. Soc. Trans. 31, 181–190.
Stevens, D., Wallis, R., 1991. The Clyde field, block 30/17b, UK North Sea. 14. Geological

Society, London, Memoirs, pp. 279–285.
Stricker, S., Jones, S., 2016. Enhanced Porosity Preservation by Pore Fluid Overpressure and Chlorite Grain Coatings in the Triassic Skagerrak, Central Graben. vol. 435. Geological Society special publications, North Sea, UK, pp. 321–341.
Stricker, S., Jones, S.J., Sathar, S., Bowen, L., Oxtoby, N., 2016. Exceptional reservoir quality in HPHT reservoir settings: examples from the skagerrak formation of the heron cluster, North Sea, UK. Mar. Petrol. Geol. 77, 198–215.
Swarbrick, R., Osborne, M., Grunberger, D., Yardley, G., Macleod, G., Aplin, A., Larter, S., Knight, I., Auld, H., 2000. Integrated study of the judy field (block 30/7a)—an overpressured Central North Sea oil/gas field. Mar. Petrol. Geol. 17, 993–1010.
Swarbrick, R., Seldon, B., Mallon, A., 2005. Modelling the Central North Sea pressure history. Geol. Soc. Lond. Petrol. Geol. Conf. series 6, 1237–1245.
Swarbrick, R.E., Lahann, R.W., O'Connor, S.A., Mallon, A.J., 2010. Role of the chalk in development of deep overpressure in the Central North Sea. Geol. Soc. Lond. Petrol. Geol. Conf. series 7, 493–507.
Tada, R., Maliva, R., Siever, R., 1987. A new mechanism for pressure solution in porous quartzose sandstone. Geochem. Cosmochim. Acta 51, 2295–2301.
Tada, R., Siever, R., 1989. Pressure solution during diagenesis. Annu. Rev. Earth Planet Sci. 17, 89–118.
Taylor, T.R., Giles, M.R., Hathon, L.A., Diggs, T.N., Braunsdorf, N.R., Birbiglia, G.V., Kittridge, M.G., Macaulay, C.I., Espejo, I.S., 2010. Sandstone diagenesis and reservoir quality prediction: models, myths, and reality. AAPG Bull. 94, 1093–1132.
Taylor, T.R., Kittridge, M.G., Winefield, P., Bryndzia, L.T., Bonnell, L.M., 2015. Reservoir quality and rock properties modeling–Triassic and Jurassic sandstones, greater Shearwater area, UK Central North Sea. Mar. Petrol. Geol. 65, 1–21.
Terzaghi, K., 1925. Principles of soil mechanics, IV—settlement and consolidation of clay. Eng. News Rec. 95, 874–878.
Valley, J.W., Kita, N.T., 2009. In situ oxygen isotope geochemistry by ion microprobe. MAC short course: Second. Ion Mass Spectrom. Earth Sci. 41, 19–63.
van Noort, R., Spiers, C.J., Pennock, G.M., 2008. Compaction of granular quartz under hydrothermal conditions: controlling mechanisms and grain boundary processes. J. Geophys. Res.: Solid Earth 113, 1–23.
Walderhaug, O., 1994a. Temperatures of quartz cementation in Jurassic sandstones from the Norwegian continental shelf–evidence from fluid inclusions. J. Sediment. Res. 64, 311–323.
Walderhaug, O., 1994b. Precipitation rates for quartz cement in sandstones determined by fluid-inclusion microthermometry and temperature-history modeling. J. Sediment. Res. 64, 324–333.
Walderhaug, O., 1996. Kinetic modeling of quartz cementation and porosity loss in deeply buried sandstone reservoirs. AAPG Bull. 80, 731–745.
Walderhaug, O., 2000. Modeling quartz cementation and porosity in Middle jurassic brent group sandstones of the kvitebjørn field, northern North Sea. AAPG Bull. 84, 1325–1339.
Walderhaug, O., Lander, R., Bjørkum, P., Oelkers, E., Bjørlykke, K., Nadeau, P., 2000. Modelling quartz cementation and porosity in reservoir sandstones: examples from the Norwegian continental shelf. In: Worden, R., Morad, S. (Eds.), Quartz Cementation in Sandstones. vol. 29. Special Publication International Association of Sedimentologists, pp. 39–49.
Waldschmidt, W.A., 1941. Cementing materials in sandstones and their probable influence on migration and accumulation of oil and gas. AAPG (Am. Assoc. Pet. Geol.) Bull. 25, 1839–1879.
Warren, E., Smalley, P., Howarth, R., 1994. Compositional variations of North Sea formation waters. North Sea Form. Waters Atlas 119–140.
Weyl, P.K., 1959. Pressure solution and the force of crystallization: a phenomenological theory. J. Geophys. Res. 64, 2001–2025.
Wilkinson, M., Haszeldine, R.S., 2011. Oil charge preserves exceptional porosity in deeply buried, overpressured, sandstones: central North Sea, UK. J. Geol. Soc. 168, 1285–1295.
Wilkinson, M., Haszeldine, R.S., Fallick, A.E., 2006. Hydrocarbon filling and leakage history of a deep geopressured sandstone, Fulmar Formation, United Kingdom North Sea. AAPG Bull. 90, 1945–1961.
Worden, R.H., Armitage, P., Butcher, A., Churchill, J., Csoma, A., Hollis, C., Lander, R., Omma, J., 2018a. Petroleum reservoir quality prediction: overview and contrasting approaches from sandstone and carbonate communities. Geol. Soc. Lond. Spec. Publ. 435 SP435. 421.
Worden, R.H., Bukar, M., Shell, P., 2018b. The effect of oil emplacement on quartz cementation in a deeply buried sandstone reservoir. AAPG (Am. Assoc. Pet. Geol.) Bull. 102, 49–75.
Worden, R.H., Morad, S., 2000. Quartz Cementation in Oil Field Sandstones: a Review of the Key Controversies. Quartz cementation in sandstones, Special publications of international association of sedimentologists, pp. 1–20 29.
Worden, R.H., Oxtoby, N.H., Smalley, P.C., 1998. Can oil emplacement prevent quartz cementation in sandstones? Petrol. Geosci. 4, 129–137.